bioRxiv preprint doi: https://doi.org/10.1101/2021.08.06.455450; this version posted August 8, 2021. The copyright holder for this preprint (which was not certified by peer review) is the author/funder, who has granted bioRxiv a license to display the preprint in perpetuity. It is made available under aCC-BY-NC-ND 4.0 International license.

Comparative untargeted metabolomic profiling of induced mitochondrial fusion in pancreatic cancer

Nicholas D. Nguyen[1,†], Meifang Yu[1,†], Vinit Y. Reddy[1], Ariana Acevedo-Diaz[1], Enzo C. Mesarick[1], Joseph Abi Jaoude[1], Min Yuan[2], John M. Asara[2,3], and Cullen M. Taniguchi [2,*]

[1] Department of Radiation Oncology, The University of Texas, MD Anderson Cancer Center, Houston, TX 77030, USA
[2] Division of Signal Transduction, Beth Israel Deaconess Medical Center, Boston, MA 02215, USA
[3] Department of Medicine, Harvard Medical School, Boston, MA 02115, USA

† These authors contributed equally to this work.

* To whom correspondence should be addressed:
Cullen M. Taniguchi, MD, PhD
The University of Texas MD Anderson Cancer Center
Division of Radiation Oncology
1515 Holcombe Blvd., Unit 1050
Houston, TX 77030-4000
T: 713-745-5269
ctaniguchi@mdanderson.org

Data & Resource Sharing: Data, materials, and reagents will be made available to other researchers upon request.

bioRxiv preprint doi: https://doi.org/10.1101/2021.08.06.455450; this version posted August 8, 2021. The copyright holder for this preprint (which was not certified by peer review) is the author/funder, who has granted bioRxiv a license to display the preprint in perpetuity. It is made available under aCC-BY-NC-ND 4.0 International license.

Abstract

Mitochondria are dynamic organelles that constantly alter their shape through the recruitment of specialized proteins, like mitofusin-2 (Mfn2) and dynamin-related protein 1 (Drp1). Mfn2 induces the fusion of nearby mitochondria, while Drp1 mediates mitochondrial fission. We previously found that the genetic or pharmacological activation of mitochondrial fusion was tumor suppressive against pancreatic ductal adenocarcinoma (PDAC) in several model systems [1]. The mechanisms of how these different inducers of mitochondrial fusion reduce pancreatic cancer growth are still unknown. Here, we characterized and compared the metabolic reprogramming of these three independent methods of inducing mitochondrial fusion in KPC cells: overexpression of Mfn2, genetic editing of Drp1, or treatment with leflunomide. We identified significantly altered metabolites via robust, orthogonal statistical analyses and found that mitochondrial fusion consistently produces alterations in the metabolism of amino acids. Our unbiased methodology revealed that metabolic perturbations were similar across all these methods of inducing mitochondrial fusion, proposing a common pathway for metabolic targeting with other drugs.

Keywords: mitochondrial morphology; fusion, fission; mitofusin-2; leflunomide; pancreatic cancer; metabolomic reprogramming; metabolomics

bioRxiv preprint doi: https://doi.org/10.1101/2021.08.06.455450; this version posted August 8, 2021. The copyright holder for this preprint (which was not certified by peer review) is the author/funder, who has granted bioRxiv a license to display the preprint in perpetuity. It is made available under aCC-BY-NC-ND 4.0 International license.

Introduction

Pancreatic ductal adenocarcinoma (PDAC) relies on mitochondrial respiration through remodeling of the electron transport chain in order to sustain its proliferative abilities [2,3]. We and others have found that morphological changes in mitochondria can alter their function [1,4]. Mitochondria undergo fusion and fission in response to external stimuli to optimize metabolic functions and to promote turnover of damaged organelles through mitophagy [5]. This balance between mitochondrial fusion and fission is regulated by two key molecules: mitofusin-2 (Mfn2) and dynamin-related protein 1 (Drp1). As its name suggests, Mfn2 directs the fusion of outer membranes in adjacent mitochondria whereas Drp1 aggregates to the surface of elongated networks, constricting the mitochondrial membranes until they break apart through the process of mitochondrial fission.

Pancreatic cancer cells often display aberrations of mitochondrial dynamics in favor of mitochondrial fission [1,6], where these organelles take on a fragmented appearance, which appears to be a KRAS-dependent phenomenon [7]. We previously demonstrated that this overactive mitochondrial fission could be therapeutically targeted by disrupting Drp1, increasing expression of Mfn2 genetically, or with the use of leflunomide [1]. The net effect of these three interventions promoted mitochondrial fusion, which curbed oxidative phosphorylation (OXPHOS), thereby suppressing tumor growth in pancreatic cancer [1]. However, the metabolic mechanism by which mitochondrial fusion reduced PDAC growth is still unknown.

To understand how mitochondrial fusion alters the cellular metabolism of PDAC, we performed an unbiased comparative metabolomic analysis between three different methods of inducing mitochondrial fusion: (1) genetically inducing fusion

bioRxiv preprint doi: https://doi.org/10.1101/2021.08.06.455450; this version posted August 8, 2021. The copyright holder for this preprint (which was not certified by peer review) is the author/funder, who has granted bioRxiv a license to display the preprint in perpetuity. It is made available under aCC-BY-NC-ND 4.0 International license.

using a tetracycline-inducible system to overexpress Mfn2 (Tet-On Mfn2), (2) directly inhibiting the decomposition of mitochondrial fusion through genetically knocking out Drp1 using CRISPR (sgDrp1), and (3) pharmacologically inducing fusion through treatment with leflunomide. We found common metabolic pathways between these different methods of inducing mitochondrial fusion, suggesting areas for metabolic intervention to further optimize this therapeutic target.

Results

Mitochondrial Fusion Distinctly Alters PDAC Metabolome

We created isogenic cell lines derived from murine KPC pancreatic tumors with proven mitochondrial fusion [8]. Tet-On Mfn2 cells express Mfn2 upon exposure to low-doses of doxycycline, which induces mitochondrial fusion compared to doxy-negative controls. We also produced cells with predominantly fused mitochondria by CRISPR-mediated abrogation of Drp1 or treatment with Leflunomide (Figure 1). We extracted metabolites from each cell line in a minimum of five biological replicates along with isogenic controls and subjected them to mass spectrometric analysis after steady state metabolite collection using a well-established methanol extraction method [9,10].

Liquid chromatography tandem mass spectrometry (LC-MS/MS) analysis quantified the relative concentration levels of 296 distinct metabolites for each of the cells. To understand the metabolites more closely correlated with mitochondrial fusion, we subjected the data to stringent filters and normalized the datasets to the control of each experimental group. Supervised partial least-squares discriminant analysis (PLS-DA) and unsupervised principal component analysis (PCA) revealed

bioRxiv preprint doi: https://doi.org/10.1101/2021.08.06.455450; this version posted August 8, 2021. The copyright holder for this preprint (which was not certified by peer review) is the author/funder, who has granted bioRxiv a license to display the preprint in perpetuity. It is made available under aCC-BY-NC-ND 4.0 International license.

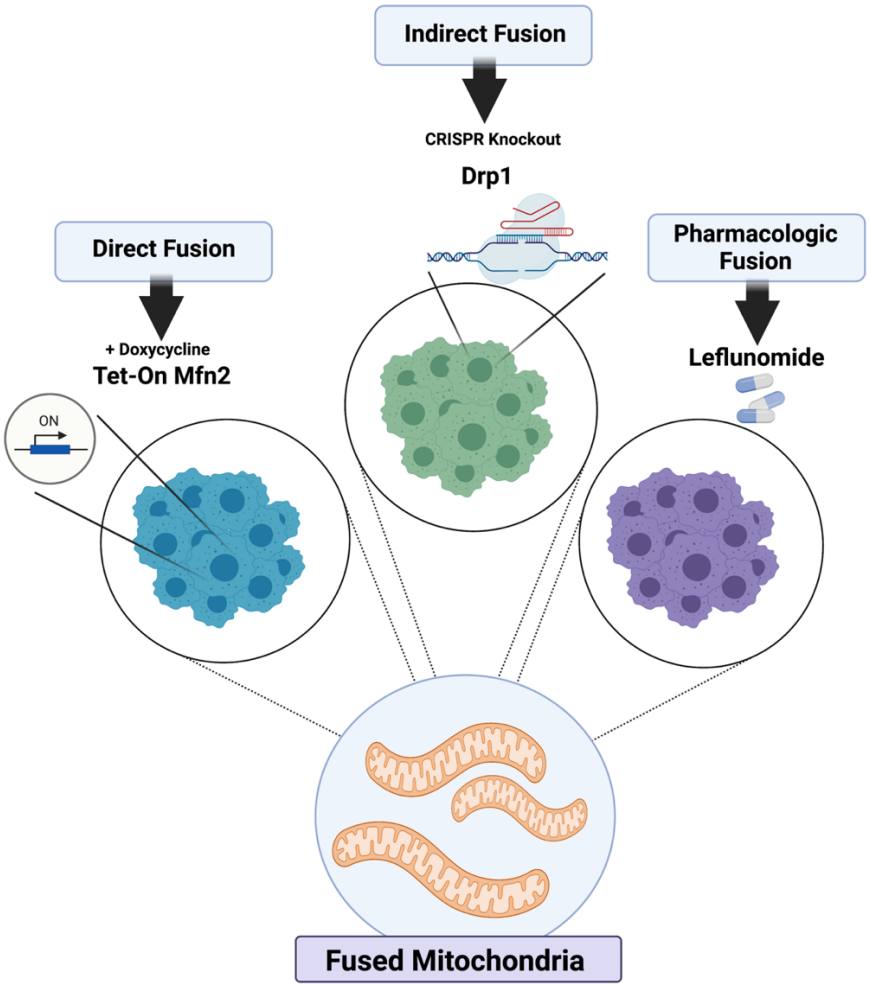

Figure 1. Models of mitochondrial fusion induction. KPC cells were genetically modified to directly overexpress Mfn2 in a tetracycline-inducible manner, indirectly fuse through CIRSPR knockout of Drp1, and pharmacologically fuse after treatment with Leflunomide.

distinct clustering between the induced mitochondrial fusion groups (n = 6) and their respective controls (n = 6, Figure 2A and 2B). Further hierarchical clustering using a euclidean distance and ward clustering algorithm revealed that individual replicates for each treatment group clustered together (Figure 2C). Overall, a total of 14 significantly altered metabolism pathways were shared between the Tet-On Mfn2, sgDrp1, and pharmacologic treated Leflunomide groups (Table 1). Metabolic super-pathways regulating amino acids and nucleotides were most consistently altered by the induction of mitochondrial fusion, compared to individual controls (Figure 2C).

bioRxiv preprint doi: https://doi.org/10.1101/2021.08.06.455450; this version posted August 8, 2021. The copyright holder for this preprint (which was not certified by peer review) is the author/funder, who has granted bioRxiv a license to display the preprint in perpetuity. It is made available under aCC-BY-NC-ND 4.0 International license.

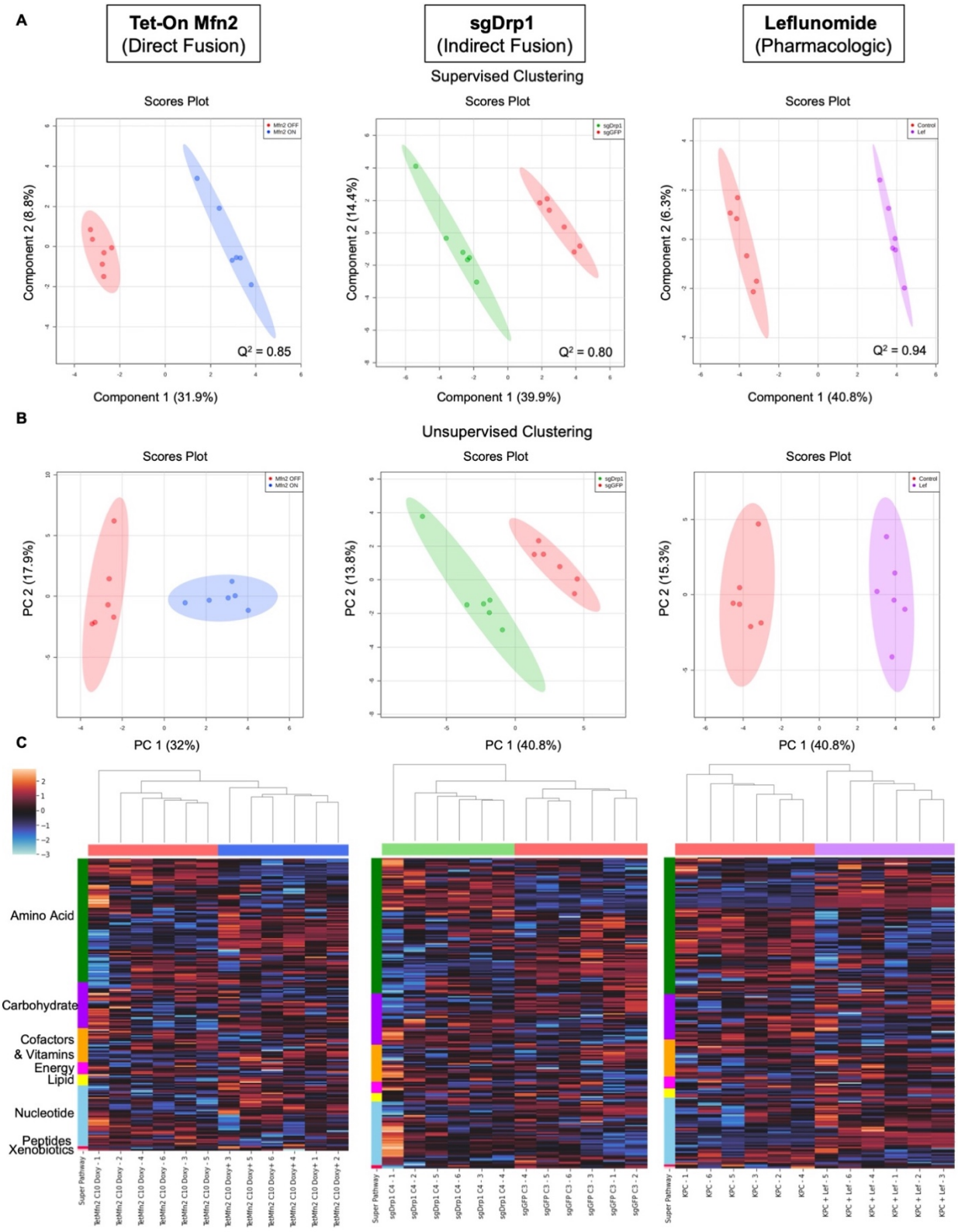

Figure 2. Multivariate clustering reveals distinct separation after inducing mitochondrial fusion when compared to controls. (A) Supervised PLS-DA and (B) unsupervised PCA score plots of Tet-On Mfn2 (blue), sgDrp1 (green), and Leflunomide (purple) treated KPC cells with respect to their corresponding controls (red). (C) Heatmap with unsupervised hierarchical clustering of affected super pathways across Tet-On Mfn2 (blue), sgDrp1 (green), and Leflunomide (purple). Both unsupervised and supervised clustering methods revealed a distinct separation between each method of fusion induction and its respective control. Predictive power of PLS-DA in component 1 represented by Q^2 = 0.85 for Tet-On Mfn2, Q^2 = 0.80 for sgDrp1, and Q^2 = 0.94 for Leflunomide.

Table 1. Common altered metabolic pathways from initial metabolite set across pathways supporting mitochondrial fusion. Pathway analysis included only pathways with an FDR < 0.05, impact > 0.25, and more than 20% of the metabolites in the pathway affected.

Pathway Name	Tet-On Mfn2 (Direct Fusion)				sgDrp1 (Indirect Fusion)				Leflunomide (Pharmacologic)			
	Percent Affected	Differentiated Metabolites	FDR	Impact	Percent Affected	Differentiated Metabolites	FDR	Impact	Percent Affected	Differentiated Metabolites	FDR	Impact
Pyrimidine Metabolism	64.10%	25/39	3.39E-04	0.82144	64.10%	25/39	0.0059471	0.7458	64.10%	25/39	2.43E-09	0.43244
Arginine Biosynthesis	78.57%	11/14	4.69E-04	0.80203	85.71%	12/14	0.0059057	0.6875	92.86%	13/14	3.73E-06	0.75
Pentose Phosphate Pathway	59.09%	13/22	0.0011839	0.7583	63.64%	14/22	9.65E-05	0.7931	63.64%	14/22	0.050181	0.65904
Alanine, Aspartate, and Glutamate Metabolism	57.14%	16/28	6.00E-05	0.73077	64.29%	18/28	8.16E-06	0.75	64.29%	18/28	2.43E-09	0.475
Glycolysis / Gluconeogenesis	50.00%	13/26	0.094261	0.64288	53.85%	14/26	8.16E-06	0.54283	53.85%	14/26	0.0061775	0.7797
Synthesis and Degradation of Ketone Bodies	40.00%	2/5	0.06157	0.6	100.00%	5/5	3.72E-05	1	60.00%	3/5	0.0057862	0.875
Glyoxylate and Dicarboxylate Metabolism	34.38%	11/32	0.094261	0.55557	43.75%	14/32	9.40E-06	0.3846	34.38%	11/32	1.67E-04	0.7931
Citrate Cycle (TCA cycle)	50.00%	10/20	0.058038	0.51326	65.00%	13/20	7.97E-06	0.62071	60.00%	12/20	6.00E-06	0.30768
Purine Metabolism	43.94%	29/66	6.00E-05	0.48314	51.52%	34/66	0.0015302	0.68176	50.00%	33/66	6.00E-06	0.66668
Arginine and Proline Metabolism	36.84%	14/38	1.07E-04	0.46873	39.47%	15/38	8.16E-06	0.45	36.84%	14/38	0.0039372	0.55174
Nicotinate and Nicotinamide Metabolism	53.33%	8/15	0.0016517	0.46053	53.33%	8/15	0.11317	0.57144	60.00%	9/15	5.65E-04	0.71428
Amino Sugar and Nucleotide Sugar Metabolism	24.32%	9/37	0.098051	0.43431	24.32%	9/37	5.33E-04	0.26088	24.32%	9/37	0.063576	0.54283
Glutathione Metabolism	32.14%	9/28	2.89E-05	0.34576	35.71%	10/28	7.08E-06	0.43244	35.71%	10/28	0.017389	0.26088
Pyruvate Metabolism	31.82%	7/22	0.16459	0.2509	45.45%	10/22	8.16E-06	0.48149	31.82%	7/22	2.10E-04	0.37038

Notably, the following three Amino Acid pathways were significantly altered in the mitochondrial fusion cohorts compared to controls: arginine biosynthesis (FDR < 0.01, Impact > 0.68, and Percent Affected > 78.5%), alanine, aspartate, and glutamate metabolism (FDR < 0.0001, Impact > 0.47, and Percent Affected > 57.1%), and glutathione metabolism (FDR < 0.05, Impact > 0.26, and Percent Affected > 32.1%, Table 1). Pyrimidine and purine metabolism were the two nucleotide sub-pathways that were significantly altered after inducing mitochondrial fusion (FDR < 0.01, Impact > 0.43, Percent Affected = 64.1% and FDR < 0.01, Impact > 0.48, Percent Affected > 43.9% respectively, Table 1). We also observed significant changes in several carbohydrate metabolism sub-pathways, including the pentose phosphate pathway (PPP), glycolysis/gluconeogenesis, the citrate cycle (TCA cycle), pyruvate metabolism, and amino sugar and nucleotide sugar metabolism (Table 1). The full unfiltered pathway analysis for Tet-On Mfn2, sgDrp1, and Leflunomide treated KPC cells can be found in Figure 3 and Table S1.

Identification of Significantly Differentiated Metabolites

From this, we found that 75 out of 234 metabolites in Tet-On Mfn2, 54 out of 245 metabolites in the sgDrp1, and 74 out of 233 metabolites in the leflunomide treated groups were altered (both up-and-downregulated) compared to controls. As represented in their corresponding volcano plots, since LC-MS/MS was unable to detect many metabolites with a fold change greater than 2, we repeated our analysis with a lower stringency threshold, considering all significant metabolites based on an FDR < 0.05 in our initial univariate analysis (Figure 4A). A full list of discriminant metabolites identified via Student's *t*-test can be found in Table S2A-C.

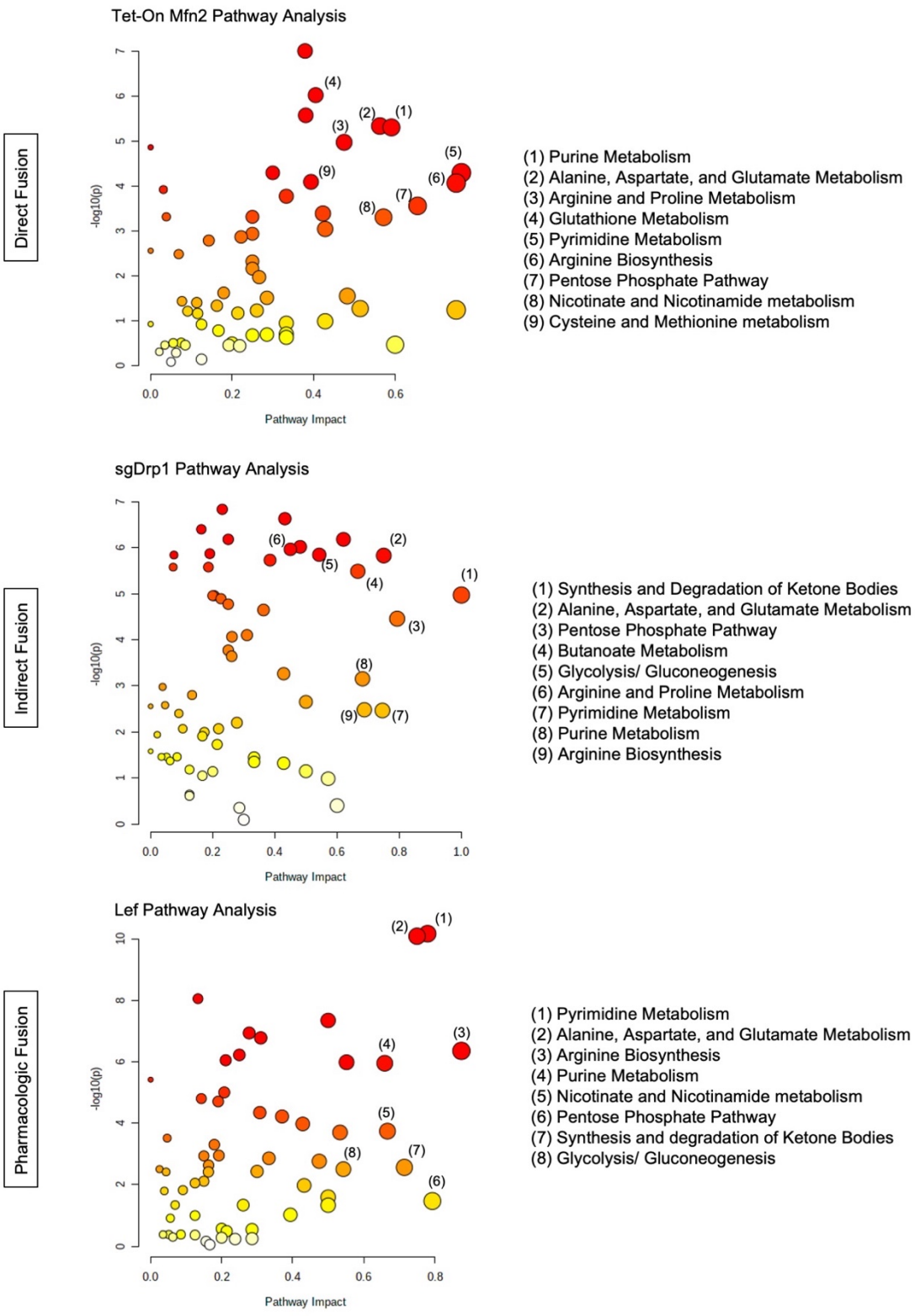

Figure 3. Total pathway analysis of filtered metabolites reveals similar impact of Amino Acid, Nucleotide, and Carbohydrate metabolism pathways as a function of mitochondrial fusion: Tet-On Mfn2 (direct), sgDrp1 (indirect), and leflunomide treatment (pharmacologic).

In order to ensure robustness in our feature selection process, we further developed three different pairwise models to identify metabolite markers for each group: a significance analysis of microarray (SAM) [11], PLS-DA variable importance in projection (VIP) [12], and a random forest (RF) [13] classification model. SAM identified 73 out of 234 metabolites in the Tet-On Mfn2 induced fusion group, 71 out of 245 metabolites in the indirect fusion group, and 74 out of 233 metabolites in the Leflunomide treated group as significantly altered based on an FDR < 0.05 and a corresponding delta of 0.39, 0.38, and 0.32 for the Tet-On Mfn2, sgDrp1, and Leflunomide groups respectively (Figure 4B). The full list of discriminant metabolites identified by SAM can be found in Table S3A-C.

Using our PLS-DA model, a VIP score greater than 1.0 [11] across all 5 principal components was used as a cutoff to identify discriminant metabolites after induction of mitochondrial fusion. From our original filtered metabolite set, we detected 83, 72, and 59 potential metabolites of interest in our Tet-On Mfn2, sgDrp1, and Leflunomide treated groups accordingly (Figure 4C and Table S4A-C). Moreover, permutation testing of 2000 repeats yielded a *P*-value = 0.001, suggesting that the separation exhibited by our PLS-DA model was not due to overfitting. We then performed leave-one-out cross validation [14] of the models and found that they had a predictive power 85% for Tet-On Mfn2, 80% for sgDrp1, and 94% for Leflunomide induced fusion.

To account for potential overfitting and potential bias from our previous models, we also developed an RF classification model for each group using MetaboAnalyst 5.0. For each RF model, we generated 500 trees to control for potential correlations

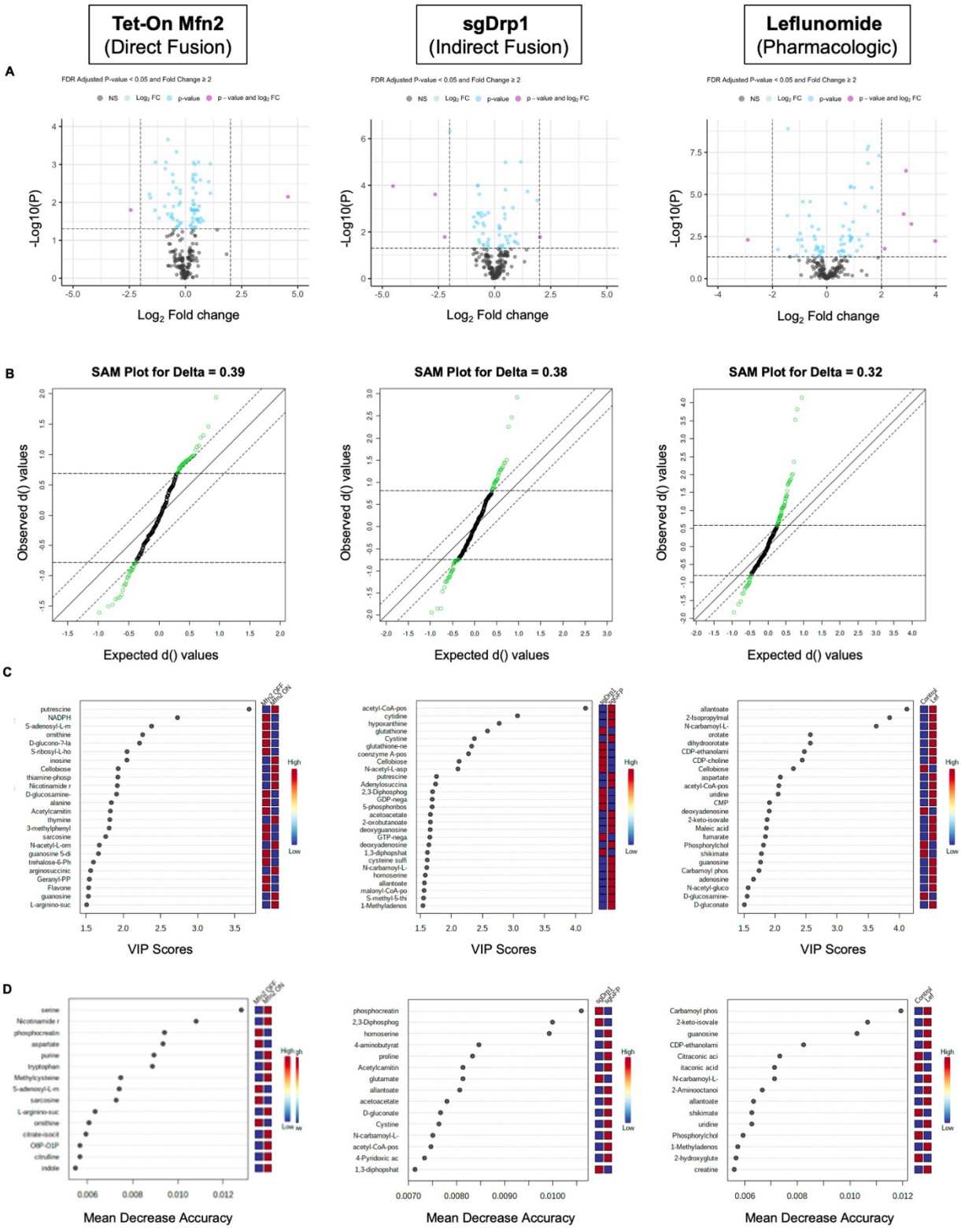

Figure 4. Statistical methods to identify differentially expressed metabolites after inducing mitochondrial fusion. (A) univariate Student's *t*-test, FDR-adjusted *P*-value < 0.05, (B) SAM, FDR < 0.05, (C) PLS-DA, VIP score < 1.0, (D) RF model, Mean Decrease Accuracy > 0.

between metabolites and subsequently measured a variable permutation importance score for each metabolite represented as the mean decrease accuracy (MDA) value. An MDA value approximates the amount that our model decreases in accuracy if the variable was taken out of the model [13]. Accordingly, we classified metabolites with MDA > 0 as discriminant and included them for pathway analysis. From our models, we identified 87 total discriminant metabolites in both the Tet-On Mfn2 and sgDrp1 groups and 81 total discriminant metabolites in the Leflunomide treated group (Figure 4D and Table S5A-C).

From our four statistical models, we combined the lists of significantly altered metabolites that contributed to each respective condition of induced mitochondrial fusion and only considered the overlap between all four lists for a definitive pathway analysis. This improved the robustness of our data analysis and further increased confidence in the identified metabolite markers for mitochondrial fusion in PDAC. As a result, we uncovered 48 unique identifier metabolites for direct fusion by Tet-On Mfn2 (Table 2), 38 unique identifier metabolites for indirect fusion by CRISPR knockout of Drp1 (Table 3), and 47 unique identifier metabolites for pharmacologic fusion by Leflunomide (Table 4).

Table 2. Discriminant metabolites identified after induction of Mfn2**.** Test statistics calculated for significantly altered metabolites overlapped across the univariate Student's *t*-test, SAM, PLS-DA, and RF analysis.

Sample Name	Fold Change	Univariate FDR	VIP Score (Comp 1)	Mean Decrease Accuracy (MDA)	SAM FDR
CDP	0.68666	0.027827	1.2867	0.00066667	0.032116
Carbamoyl Phosphate	1.2514	0.02605	1.0081	0.0018	0.050381
Asparagine	1.2635	0.011257	1.0645	0.0034	0.037373
D-Glucosamine-1-Phosphate	0.44312	0.02605	1.9094	0.0023333	0.01374
S-Adenosyl-L-Methioninamine	0.32905	0.006065	2.3789	0.0022667	0.004837

Table 2. *Cont.*

Sample Name	Fold Change	Univariate FDR	VIP Score (Comp 1)	Mean Decrease Accuracy (MDA)	SAM FDR
2-Dehydro-D-Gluconate	0.68566	0.002861	1.3958	0.0099333	0.02345
Indole	1.3634	0.002861	1.2668	0.003	0.028201
Citrulline	1.2704	0.001842	1.1353	0.0055333	0.031391
GTP	1.3369	0.015975	1.1558	0.001	0.035478
Arginosuccinic acid	1.584	0.002567	1.5611	0.0059333	0.014225
GMP	1.4193	0.01588	1.3029	0.0018	0.02992
2-Aminooctanoic acid	0.66975	0.001842	1.4631	0.0036	0.018513
Arginine	1.2535	0.002277	1.1008	0.0034	0.033201
Purine	1.2645	0.004142	1.0987	0.005	0.034076
NADPH	0.1846	0.01588	2.729	0.0026333	0.004837
O8P-O1P	1.3778	0.005756	1.2761	0.0065333	0.029076
L-Arginino-Succinate	1.4956	0.000871	1.5079	0.0084429	0.01374
Alanine	0.54833	0.000871	1.839	0.0148	0.004837
5-Phosphoribosyl-1-Pyrophosphate	1.5979	0.025893	1.4581	0.00066667	0.027951
S-Ribosyl-L-Homocysteine	0.3906	0.016169	2.049	0.0031333	0.00916
Acetylcarnitine DL	0.53482	0.001287	1.8265	0.0032667	0.004837
2-Hydroxy-2-Methylbutanedioic acid	1.402	0.01588	1.2822	0.0023333	0.02992
Glutathione Disulfide	1.314	0.019782	1.0971	0.0089333	0.037373
Phenylalanine	1.2826	0.000891	1.1717	0.012333	0.029179
dTMP	1.118	0.020287	1.4411	0.0056	0.027951
NADH	1.246	0.012535	1.4343	0.00066667	0.026043
Nicotinamide Ribotide	2.0503	0.002861	1.9196	0.0023333	0.004837
Uridine	1.4011	0.027827	1.2289	0.0014	0.034076
Indoleacrylic acid	1.3169	0.011539	1.168	0.0048	0.034076
Tryptophan	1.374	0.001842	1.3031	0.0067333	0.026043
3-Phosphoglycerate	0.68917	0.012848	1.3362	0.0051333	0.029076
N-Acetyl-Glucosamine	0.66265	0.024296	1.3427	0.0013	0.02992
Sarcosine	0.58198	0.000223	1.7628	0.0058	0.004837
Tyrosine	1.2589	0.008888	1.0657	0.011667	0.037231
Aspartate	0.75934	0.000467	1.25	0.0051333	0.026043
D-Glucono-1,5-Lactone-6-Phosphate	0.33822	0.007515	2.2168	0.0036	0.004837
Methylcysteine	1.3329	0.001001	1.2559	0.002	0.026043
Glycerophosphocholine	1.3214	0.016098	1.1381	0.0042667	0.035478
Putrescine	23.644	0.007136	3.6927	0.0033333	0
Ornithine	0.39436	0.000871	2.2593	0.0063333	0.004837
Trehalose-6-Phosphate	0.57804	0.020287	1.5976	0.0010667	0.02345
Carnitine	0.74822	0.004142	1.2306	0.0052667	0.02927
Pantothenate	1.4739	0.016169	1.3268	0.0039333	0.029312
Serine	1.2597	0.002567	1.1152	0.0044	0.032885
Guanosine	1.721	0.030407	1.5297	0.0008	0.026043
Inosine	2.1501	0.000967	2.0471	0.0099333	0.004837
Orotidine-5-Phosphate	1.499	0.02791	1.3552	0.0023333	0.02992
Thiamine-Phosphate	2.1668	0.005756	1.9265	0.0058	0.007195

Table 3. Discriminant metabolites identified after deletion of Drp1. Test statistics calculated for significantly altered metabolites overlapped across the univariate Student's *t*-test, SAM, PLS-DA, and RF analysis.

Sample Name	Fold Change	Univariate FDR	VIP Score (Comp 1)	Mean Decrease Accuracy (MDA)	SAM FDR
Betaine	0.664180	0.002147	1.4133	0.0086	0.007697
4-Pyridoxic acid	0.725180	0.037598	1.1296	0.0013333	0.033019
Phosphocreatine	1.316600	0.000906	1.1742	0.0052667	0.014145
Aminoimidazole Carboxamide Ribonucleotide	0.630100	0.028337	1.4028	0.0016667	0.014111
Glutathione	3.742600	0.000442	2.5826	0.0062667	0
Glutathione	3.742600	0.000182	2.3268	0.0049333	0
Acetoacetate	0.596270	0.000101	1.662	0.0072	0.004233
2-Oxobutanoate	0.593130	0.000101	1.6618	0.0033333	0.004233
GTP	1.920100	0.026715	1.6525	0.0042667	0.007697
N-Carbamoyl-L-Aspartate	0.821900	0.001503	1.6041	0.0068	0.005064
D-Gluconate	0.724880	0.005425	1.2393	0.0022667	0.015196
Homoserine	0.598390	0.00421	1.5808	0.0054667	0.005681
Acetyl-CoA	0.043581	0.000107	4.1582	0.0039333	0
N-Acetyl-L-Aspartic acid	2.249000	9.87E-06	2.1057	0.0046667	0
Adenylosuccinate	0.533700	0.006098	1.7461	0.0057667	0.005064
GDP	2.053600	0.03156	1.6927	0.0043333	0.007697
5-Phosphoribosyl-1-Pyrophosphate	1.758200	0.000906	1.6914	0.0022667	0.00449
Cytidine	0.159910	0.000242	3.0649	0.0071333	0
S-Ribosyl-L-Homocysteine	1.415700	0.015789	1.2606	0.00066667	0.016006
Acetylcarnitine DL	0.666230	0.001503	1.4281	0.0023333	0.007362
N-Acetyl-Glutamine	1.607500	0.014761	1.4623	0.0017333	0.01127
Deoxyguanosine	0.562700	0.003641	1.6583	0.0024667	0.005064
Betaine Aldehyde	0.702120	0.00421	1.3118	0.0048	0.012147
1,3-Diphopshateglycerate	1.842500	0.025568	1.6151	0.0041333	0.00898
Homocysteine	1.377000	0.001738	1.2676	0.0057333	0.012147
dAMP	1.372600	0.002658	1.2376	0.0054	0.014111
D-Glucono-1,5-Lactone-6-Phosphate	0.700130	0.011761	1.2703	0.0018	0.015485
Homocysteic acid	0.616910	0.021676	1.4179	0.0014667	0.013178
Cystine	0.214900	0.016467	2.3705	0.0048	0.003848
4-Aminobutyrate	0.741390	0.001858	1.2177	0.0078667	0.014111
Putrescine	0.528260	0.00226	1.7602	0.0076	0.00449
Ornithine	1.405100	1.04E-05	1.3596	0.0077667	0.005064
coenzyme A	4.070400	0.016467	2.2758	0.0041333	0.004233
2,3-Diphosphoglyceric acid	1.926400	0.012063	1.6976	0.0048	0.00558
Hypoxanthine	0.251200	4.76E-07	2.7704	0.0075333	0

Table 3. *Cont.*

Sample Name	Fold Change	Univariate FDR	VIP Score (Comp 1)	Mean Decrease Accuracy (MDA)	SAM FDR
Citrate	1.398700	0.000156	1.329	0.0092667	0.007362
Allantoate	0.624710	0.000242	1.5666	0.001	0.004737
1-Methyladenosine	0.614980	0.00169	1.5425	0.0023333	0.005064

Table 4. Discriminant metabolites identified after treatment with Leflunomide. Test statistics calculated for significantly altered metabolites overlapped across the univariate Student's *t*-test, SAM, PLS-DA, and RF analysis.

Sample Name	Fold Change	Univariate FDR	VIP Score (Comp 1)	Mean Decrease Accuracy (MDA)	SAM FDR
Citrate-Isocitrate	0.653650	2.70E-05	1.1599	0.003967	0.007573
CDP	1.771000	0.001233	1.3036	0.005133	0.00732
Carbamoyl Phosphate	2.619400	5.46E-05	1.742	0.007	0.001114
Fumarate	2.787300	2.11E-08	1.8458	0.002514	0.000255
Aminoimidazole Carboxamide Ribonucleotide	0.526080	0.004786	1.3578	0.010638	0.007407
Choline	0.533840	0.011992	1.2772	0.002	0.008622
Orotate	15.739000	0.005825	2.5694	0.0008	0.000727
Thiamine Pyrophosphate	1.780700	0.002856	1.2673	0.003433	0.007573
Acetoacetate	0.586710	0.022826	1.1496	0.002267	0.015481
Phosphorylcholine	0.373280	1.28E-09	1.8143	0.011533	0.000255
Isocitrate	0.476540	0.00499	1.4156	0.002133	0.00732
Deoxyadenosine	0.288340	0.018626	1.9068	0.0009	0.005729
1-Methyladenosine	1.883400	0.003598	1.36	0.006667	0.00732
2-Aminooctanoic acid	1.811500	0.00499	1.2672	0.005743	0.007639
D-Gluconate	1.999000	3.90E-06	1.5065	0.005733	0.003395
2-Keto-Isovalerate	2.868000	1.39E-08	1.8731	0.005743	0.000255
Acetyl-CoA-Posi	4.344300	0.016695	2.0614	0.0008	0.004201
N-Carbamoyl-L-Aspartate	51.968000	2.86E-10	3.627	0.0074	0
Cellobiose	0.133540	0.00499	2.2961	0.005467	0.001019
O8P-O1P	1.511200	0.000757	1.1186	0.008533	0.00911
Thiamine-Phosphate	1.822400	0.0487	1.1472	0.0005	0.018784
Creatine	1.813900	3.86E-06	1.394	0.004333	0.00544
CDP-Ethanolamine	7.034600	0.000145	2.4725	0.005	0
Acetylcarnitine DL	1.841000	0.00338	1.2953	0.004133	0.007573
Aconitate	0.542060	2.70E-05	1.3988	0.009033	0.005729
Shikimate	0.366580	0.000181	1.7807	0.005267	0.001198
Anthranilate	1.485100	0.021202	1.0136	0.002333	0.021203

Table 4. *Cont.*

Sample Name	Fold Change	Univariate FDR	VIP Score (Comp 1)	Mean Decrease Accuracy (MDA)	SAM FDR
Uridine	3.660400	9.62E-05	2.0507	0.001143	0.000727
2-Isopropylmalic acid	81.792000	1.87E-11	3.8439	0.009533	0
CMP	3.126500	3.90E-06	1.9097	0.004067	0.000424
CDP-Choline	8.569100	0.000571	2.4383	0.0036	0.000255
Deoxyguanosine	0.507480	0.002085	1.4019	0.0026	0.00732
Citraconic acid	0.639440	0.000181	1.1726	0.004733	0.007573
N-Acetyl-Glucosamine	1.556400	0.008589	1.109	0.005467	0.01403
Glycerophosphocholine	1.606000	3.48E-05	1.2246	0.004	0.00732
2-Oxo-4-Methylthiobutanoate	0.461890	0.043799	1.4045	0.0014	0.00941
Histidinol	1.546000	0.024378	1.021	0.0032	0.021203
4-Aminobutyrate	1.947500	0.000426	1.4171	0.0046	0.006111
Dihydroorotate	7.470800	3.97E-07	2.5685	0.0076	0
UDP	1.853800	0.004218	1.3149	0.0066	0.007573
Itaconic acid	0.688280	0.000804	1.0502	0.006067	0.012297
Maleic acid	2.836300	1.41E-07	1.8604	0.0048	0.000424
dCDP	1.193600	0.00578	1.3101	0.004667	0.007639
N-Acetyl-Glucosamine-1-Phosphate	2.279300	0.00499	1.5674	0.0008	0.006463
Aspartate	3.759100	4.98E-08	2.0869	0.0108	0
Allantoate	158.36	3.66E-12	4.1202	0.0084	0
Guanosine	2.803700	0.002386	1.7677	0.005	0.003886

Targeted Pathway Analysis Distinguishes altered Metabolome after Mitochondrial Fusion

When conducting sub-pathway analysis from each list of discriminant metabolites identified via one of our four statistical models, we found that the overarching patterns observed in alterations of Amino Acid, Nucleotide, and Carbohydrate super-pathways remained similar to those of our initial untargeted sub-pathway analysis. More importantly, sub-pathway analysis from each distinct discriminant metabolite identification method appeared to yield very similar phenotypes across direct genetic fusion, indirect genetic fusion, and pharmacologic fusion (Figures S1-4 and Tables S6-9A-C). Using our overlapped discriminant metabolite list for sub-pathway analysis, we

discovered that even our more limited metabolite set was able to recapitulate these trends in metabolic repogramming in each independent method of mitochondrial fusion induction. Specifically, Amino Acid, Nucleotide, and Carbohydrate pathways were altered across all three experimental groups (Figure 5). We found eight particular sub-pathways that were considered significantly impacted after filtering the raw pathway outputs from MetaboAnalyst based on an FDR < 0.05 (Table S10A-C). These included alanine, aspartate, and glutamate metabolism (FDR < 0.0001), arginine biosynthesis (FDR < 0.0001), glutathione metabolism (FDR < 0.05), cysteine and methionine metabolism (FDR < 0.01), pyrimidine metabolism (FDR < 0.0001), purine metabolism (FDR < 0.0001), PPP (FDR < 0.001), and glycolysis/gluconeogenesis (FDR < 0.05, Table 5).

Further analysis revealed that although these pathways were considered statistically significant based on our FDR adjusted *P*-value*,* we observed that many of these pathways had a low impact and correspondingly low percentage of affected metabolites in one of the three groups. Diving deeper, arginine biosynthesis appeared to be more affected after direct fusion with Tet-On Mfn2 (Impact = 0.56, Percent Affected = 42.9%) than after indirect fusion with sgDrp1 (Impact = 0.19, Percent Affected = 14.3%) and pharmacologic fusion with Leflunomide (Impact = 0.13, Percent Affected = 21.4% Table 5). Glutathione metabolism was more heavily affected by indirect fusion (Impact = 0.27, Percent Affected = 17.9%) than direct fusion (Impact = 0.16, Percent Affected = 14.3%) and pharmacologic fusion (Impact = 0.03, Percent Affected = 3.6%). Cysteine and methionine metabolism was least impacted by Leflunomide treatment (Impact = 0.03, Percent Affected = 3.0%) followed by Drp1

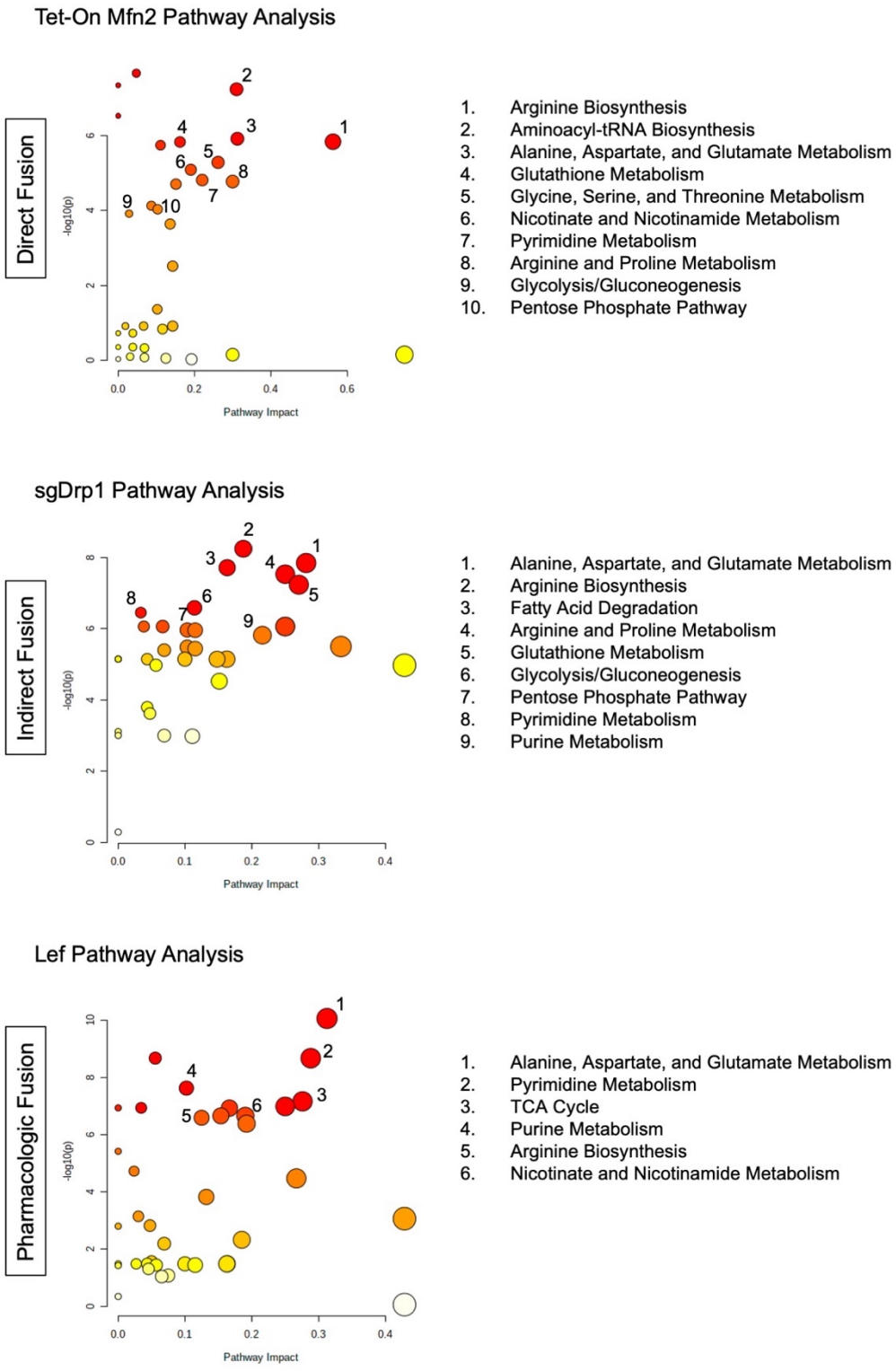

Figure 5. Pathway analysis of overlapped discriminant metabolites from direct fusion in Tet-On Mfn2, indirect fusion in sgDrp1, and pharmacologic fusion in leflunomide treated KPC cells.

knockout (Impact = 0.15, Percent Affected = 12.1%) and Mfn2 upregulation (Impact = 0.15, Percent Affected = 15.2%, Table 5). Understandably, pyrimidine metabolism was most affected by Leflunomide treatment (Impact = 0.28, Percent Affected = 25.6%) since its mechanism of action directly inhibits dihydroorotate dehydrogenase (DHODH), a crucial enzyme in the de novo pyrimidine biosynthesis pathway. Interestly, direct fusion through Tet-On Mfn2 closely mirrored Leflunomide's effect on pyrimidine metabolism, having an impact of 0.22 on the pathway with 23.1% of its metabolites altered (Table 5). Purine metabolism was most affected by indirectly inducing fusion with knockout of Drp1 (Impact = 0.22, Percent Affected = 15.2%); though, still moderately altered via direct fusion with Tet-On Mfn2 (Impact = 0.14, Percent Affected = 10.6%) and pharmacologic fusion with Leflunomide (Impact = 0.10, Percent Affected = 9.1%, Table 5). Both carbohydrate metabolism sub-pathways, PPP, and glycolysis were modestly impacted across the three groups, but knockdown of Drp1 in particular had more impact on glycolysis/gluconeogenesis (Impact = 0.11, Percent Affected = 11.5%), supporting recent findings that Drp1 promotes metabolic changes through glycolysis to drive PDAC tumorigenesis (Table 5) [7,15]. The main pathway that had an impact greater than 0.28 across the Tet-On Mfn2, sgDrp1, and Leflunomide groups was alanine, aspartate, and glutamate metabolism with more than 21.4% of the pathway appearing significantly altered (Table 5).

Table 5. Significantly altered pathways from overlapped discriminant metabolite sets.

Pathway Name	Percent Affected	Differentiated Metabolites	FDR	Impact
		Tet-On Mfn2 (Direct Fusion)		
Beta-Alanine Metabolism	9.52%	2/21	6.74E-07	0.04762
Aminoacyl-tRNA Biosynthesis	16.67%	8/48	6.74E-07	0.31033

Table 5. *Cont.*

Pathway Name	Percent Affected	Differentiated Metabolites	FDR	Impact
		Tet-On Mfn2 (Direct Fusion)		
Alanine, Aspartate, and Glutamate Metabolism*	28.57%	8/28	7.36E-06	0.3125
Arginine Biosynthesis*	42.86%	6/14	7.36E-06	0.5625
Glutathione Metabolism*	14.29%	4/28	7.36E-06	0.16216
Pantothenate and CoA Biosynthesis	15.79%	3/19	7.85E-06	0.11112
Glycine, Serine, and Threonine Metabolism	17.65%	6/34	0.00002	0.26191
Nicotinate and Nicotinamide Metabolism	13.33%	2/15	2.83E-05	0.19048
Pyrimidine Metabolism*	23.08%	9/39	4.87E-05	0.22035
Arginine and Proline Metabolism	13.16%	5/38	4.88E-05	0.3
Cysteine and Methionine Metabolism*	15.15%	5/33	5.28E-05	0.15151
Amino Sugar and Nucleotide Sugar Metabolism	5.41%	2/37	0.000185	0.08696
Pentose Phosphate Pathway*	13.64%	3/22	0.000216	0.10345
Glycolysis / Gluconeogenesis*	3.85%	1/26	0.000264	0.02857
Purine Metabolism*	10.61%	7/66	0.00047	0.13634
		sgDrp1 (Indirect Fusion)		
Arginine Biosynthesis*	14.29%	2/14	2.05E-07	0.1875
Alanine, Aspartate, and Glutamate Metabolism*	21.43%	6/28	2.32E-07	0.28125
Fatty Acid Degradation	5.13%	2/39	2.32E-07	0.16327
Arginine and Proline Metabolism	15.79%	6/38	2.66E-07	0.25
Glutathione Metabolism*	17.86%	5/28	4.20E-07	0.27028
Glycolysis / Gluconeogenesis*	11.54%	3/26	1.56E-06	0.11428
Pyrimidine Metabolism*	7.69%	3/39	1.82E-06	0.0339
Nitrogen Metabolism	16.67%	1/6	2.85E-06	0.25
Pentose Phosphate Pathway*	18.18%	4/22	3.06E-06	0.10344
Glyoxylate and Dicarboxylate Metabolism	9.38%	3/32	3.06E-06	0.11538
Purine Metabolism*	15.15%	10/66	3.92E-06	0.2159
Butanoate Metabolism	26.67%	4/15	7.42E-06	0.33334

Table 5. *Cont.*

		sgDrp1 (Indirect Fusion)		
Citrate Cycle (TCA cycle)	10.00%	2/20	7.42E-06	0.10345
Propanoate Metabolism	8.70%	2/23	7.69E-06	0.11538
Cysteine and Methionine Metabolism*	12.12%	4/33	3.69E-05	0.15151
		Leflunomide (Pharmacologic)		
Alanine, Aspartate, and Glutamate Metabolism*	25.00%	7/28	3.28E-09	0.3125
Pantothenate and CoA Biosynthesis	10.53%	2/19	2.69E-08	0.05556
Pyrimidine Metabolism*	25.64%	10/39	2.69E-08	0.28815
Purine Metabolism*	9.09%	6/66	2.25E-07	0.10227
Citrate Cycle (TCA cycle)	30.00%	6/20	5.03E-07	0.27587
Valine, Leucine, and Isoleucine Biosynthesis	12.50%	1/8	5.03E-07	0.25
Aminoacyl-tRNA Biosynthesis	2.08%	1/48	5.03E-07	0.03448
Glyoxylate and Dicarboxylate Metabolism	12.50%	4/32	7.65E-07	0.15384
Nicotinate and Nicotinamide Metabolism	13.33%	2/15	7.65E-07	0.19048
Arginine Biosynthesis*	21.43%	3/14	8.20E-07	0.125
Glycine, Serine, and Threonine Metabolism	5.88%	2/34	4.87E-05	0.02381
Butanoate Metabolism	26.67%	4/15	8.19E-05	0.26667
Valine, Leucine, and Isoleucine Degradation	10.00%	4/40	0.000343	0.13208
Cysteine and Methionine Metabolism*	3.03%	1/33	0.00155	0.0303
Beta-Alanine Metabolism	9.52%	2/21	0.002936	0.04762
Pentose Phosphate Pathway*	9.09%	2/22	0.010995	0.06896
Glutathione Metabolism*	3.57%	1/28	0.04232	0.02703
Glycolysis / Gluconeogenesis*	7.69%	2/26	0.043741	0.05714

*Pathways common amongst Tet-On Mfn2, sgDrp1, and Lef treatment.

Interestingly, several pathways from this analysis were identified as specific to each independent method for mitochondrial fusion induction. We noticed that direct fusion via Tet-On Mfn2 showed distinct impact on aminoacyl-tRNA biosynthesis and glycine, serine, and threonine metabolism in the top 5 pathway hits (Figure 5). Likewise, fatty acid degradataion and the citrate cycle were specific to sgDrp1 and Leflunomide groups when considering only the top 5 pathway hits (Figure 5). Nevertheless, after mapping the significantly altered metabolic pathways identified from the KEGG database using our overlapped discriminant metabolite set exhibited that they were in fact highly interconnected (Figure S5). Alanine, aspartate, and glutamate metabolism fed into each of the previously mentioned metabolic pathways, aligning with each of our metabolic screens. Furthermore, we see that many of the pathways are interdependent among each other, suggesting that altering mitochondrial morphology from a punctate to fused state does in fact play a significant role in metabolic reprogramming in favor of curbing tumorigenesis.

Discussion

Advances in mitochondrial biology in the previous decade have opened the doors to novel means of therapeutically targeting tumorigenesis. It has been widely shown that mitochondrial respiration is essential across multiple tumor-types in order to circumvent limitations in glycolysis, actively remodeling their means for cellular energetics [3,16–18]. This is particularly true in pancreatic cancer where mitochondrial dysfunction has been found to shift the cellular bioenergetics of cells to favor OXPHOS, supporting proliferation and metastasis [19,20]. Moreover, we and others have shown that defects

in *KRAS*, the most widely mutated gene in PDAC, is characteristic of fragmented mitochondria [1,7,20]. Although more than 90% of PDAC cases are driven by oncogenic *KRAS* [21], limited advancements have been made in formulating a clinical approach to target the gene. Instead, our work provided an alternative solution, altering the phenotypic state of mitochondria driven by KRAS through Drp1, which in turn suppressed tumor growth through modulating levels of defective mitochondria and limiting OXPHOS capability in PDAC [1]. In order to gain a better understanding of the impact of shifting the status of mitochondria from fragmented to fused, we attempted to elucidate the metabolome of PDAC after three independent methods of inducing fusion. To our knowledge, this is the first comparative metabolomic study of mitochondrial fusion in pancreatic cancer to identify macroscopic pathway alterations.

Our study builds upon previous findings to better understand common metabolic perturbations from mitochondrial fusion. Here, we used three different models: a direct fusion model involving the upregulation of Mfn2 in a doxycycline-dependent manner, an indirect fusion model through the attenuation of Drp1 using CRISPR-Cas9, and a pharmacologic approach with Leflunomide, each in KPC cells. Of note, alanine, aspartate, and glutamate metabolism was the most prominent hit across all three methods of induced fusion, understandably because of its overarching position providing the precursors for the other seven identified metabolic pathways commonly altered (Figures 5 and S5). This finding further supports current working theories of tumor ability to alternatively fuel metabolism using extracellular amino acid pools, particularly, alanine, aspartate, glutamate, and asparagine, as carbon sources [10,22].

We also observed several expected alterations in nucleotide pathways downstream due to dysregulation of glycolysis and PPP that are linked to mutant KRAS activation [20,23–25] by reducing the pool of fragmented mitochondria present. Leflunomide is widely known for its direct inhibition of DHODH, an enzyme localized on the inner mitochondrial membrane, that is responsible for de novo pyrimidine biosynthesis. Interestingly, genetic modulation of mitochondrial morphology appeared to affect these pathways in a similar fashion. Tet-On Mfn2 and sgDrp1 modulated pyrimidine biosynthesis in addition to glycolysis and PPP, showing a common set of metabolic disturbances across multiple super-pathways. Ultimately, this suggests that mitochondrial fusion may actually be working in tandem with DHODH inhibition as a tumor suppressive mechanism in pancreatic cancer.

Nevertheless, future research is needed in order to fully characterize the mechanism by which mitochondrial fusion reprograms the metabolome to curb tumorigenesis. We recognize that our study follows a markedly stringent method of discriminant metabolite identification. Relative metabolite concentration readings missed at least 1 data point for more than 20% of our metabolites across all three induced fusion groups as a result of either low concentration or poor mass spectrometry signal response, potentially limiting our analysis. Methods to impute these missing values should be explored when doing an in-depth analysis of sub-pathway alterations. However, our study provides foundational evidence that mitochondrial morphology plays a notable role in metabolic reprogramming further supporting leflunomide as a novel therapeutic against PDAC due to its ability to leverage both mitochondrial fusion and DHODH inhibition.

Materials and Methods

Cell Culture

Murine KPC cells syngeneic with C57BL/6 (K8484) were a generous gift from Anirban Maitra from the University of Texas MD Anderson Cancer Center. KPC cells were grown in RPMI-1640 supplemented with 10% FBS, 2 mM GlutaMax, 1 mM sodium pyruvate, and 7 μg/mL of insulin. We previously described the generation and selection of KPC Tet-On Mfn2, sgDrp1, and sgGFP clones [1].

Untargeted Metabolomic Analysis

All metabolomic analyses were conducted under steady state conditions. KPC cell lines were grown in appropriate growth media in six replicates in 10-cm plates. Two hours before metabolite collection, cells were incubated in fresh growth media. Accordingly, replicate cell lines were plated and grown in parallel in order to control for cell growth. Cell counts from the replicate plates were used to normalize metabolite readings. After incubation in fresh growth media, 4 mL of 80% methanol that was pre-chilled to -80˚C was added, and the cell plates were immediately transferred to -80˚C to incubate overnight. The cell lysate-methanol mixture was then scraped and transferred to conical tubes on dry ice and centrifuged at 5000 g for 5 minutes. The supernatant was collected, and the process was repeated two more times after resuspending the pellet in 500 μL of chilled 80% methanol, for a total volume of 5 mL. Samples were then completely dried via speed vacuum at 30˚C. Metabolites were analyzed by LC-MS/MS as previously described [9,10].

Discriminant Metabolite Identification

From our initial 296 measured metabolites, we stringently filtered out readings that were missing any values to ensure robustness in our analysis. As a result, 79.1%, 82.8%, and 78.7% of the metabolites within the datasets remained for our Tet-On Mfn2, sgDrp1, and Leflunomide groups, respectively. Continued filtering for altered metabolites was performed using four independent statistical approaches: (1) FDR-adjusted two-sided Student's *t*-test (*P*-values < 0.05 were considered statistically significant), (2) SAM (significant metabolite features were identified at an FDR < 0.05 and corresponding delta of 0.39 for Tet-On Mfn2, 0.38 for sgDrp1, and 0.32 for Leflunomide), (3) PLS-DA variable importance in projection (VIP scores > 1.0 were considered significant for class separation), and (4) RF classification based on 500 trees (significance established at permutation importance, MDA > 0).

Two-sided Student's *t*-test characterized significant differences based on hypothesis testing of the groups' means following a normal distribution. However, since we only had an n = 6 for each group, there is the possibility that the variance in our dataset is not stable [26]. To account for this, SAM uses a nonparametric approach which does not rely on a prescribed probability distribution [27,28]. SAM processes multiple permutations of our data in order to calculate FDR values, which we are able to control using the tuning parameter delta, allowing us to define our cutoff for identification of altered metabolites [29]. PLS-DA VIP measures the importance of each variable after supervised dimensional reduction using a partial least squares projection [30,31]. Given that the average squared VIP score is 1.0, we followed the field standard of considering VIP scores greater than 1.0 as significantly altered and confirmed its predictive

probabilities using a leave-one-out cross validation method [32]. RF is a machine learning model often used for regression and classification. We tuned an RF model using bootstrap sampling to generate 500 random classification trees. Since this model only uses a subset of the available data to generate trees, we were able to robustly limit overfitting as well as potential outliers [33]. An MDA score was calculated using the unbiased out-of-bag classification error for each metabolite predictor, representing its predictive importance for the model. The reference MDA of 0 signifies that the predictor has no predictive importance in the model. Therefore, a metabolite with an MDA > 0 represents that the loss of that metabolite from the model will result in a decrease in predictive ability of the RF model, which we used as our cutoff for identifying discriminant metabolites. In order to confirm our pathway analysis findings from the discriminant metabolite lists generated from each of our statistical models, we further refined our list of metabolites by taking only those that were common across all four feature selection methods.

Pathway Analysis

Custom data mining using BioPython's KEGG API was used to collect super metabolic pathway data for hierarchical clustering similar to what has previously been described [34]. Further sub-pathway analysis was performed using MetaboAnalyst 5.0, initially on the total filtered metabolite set from the KEGG database for *mus musculus*. We used a Global Test for enrichment and out-degree centrality for topology analysis. Using the hit values from the MetaboAnalyst output, we calculated a percent affected score for each pathway to prevent identification of significantly altered pathways with

fewer than 20% of their metabolites altered. Significant sub-pathways were also filtered using an FDR adjusted *P*-value < 0.05 and impact greater than 0.25. Confirmation of sub-pathway alterations after induction of mitochondrial fusion was performed after running continued pathway analyses of each discriminant metabolite set generated from our four different statistical methods as well as our overlapped metabolite dataset.

Statistical Analysis

Data manipulation and statistical analyses were performed using MetaboAnalyst 5.0 [35], R version 4.0.2, and the Pandas, NumPy, and SciPy libraries in python 3.8. Metabolite concentration values were normalized based on the control group for each respective experimental group and log-transformed and pareto-scaled to approximate a normal distribution. 2D PCA and PLS-DA scores plots were generated using MetaboAnalyst. Heatmaps were generated with the python Seaborn package using a euclidean distance measure and ward algorithm. Volcano plots were generated using the EnhancedVolcano package from Bioconductor in R [36].

Author Contributions

Conceptualization, N.D.N., M.Y. and C.M.T.; methodology, N.D.N. and M.Y.; validation, N.D.N. , formal analysis, N.D.N.; investigation, N.D.N. and M.Y., resources, N.D.N. and M.Y.; data curation, N.D.N., M.Y., M.Y. and J.M.A.; writing —original draft preparation, N.D.N.; writing —review and editing, N.D.N., V.Y.R., E.C.M., J.A.J., and C.M.T.; visualization, N.D.N., V.Y.R., A.R., E.C.M., and J.A.J.; supervision, N.D.N., M.Y.

and C.M.T.; project administration, N.D.N. and C.M.T., funding acquisition, C.M.T. All authors have read and agreed to the published version of the manuscript.

Funding

C.M.T. was supported by funding from the following sources: the National Institutes of Health (NIH) under award number R01CA227517-01A1, the Cancer Prevention & Research Institute of Texas (CPRIT) grant RR140012, the V Foundation (V2015-22), the Sidney Kimmel Foundation, a Sabin Family Foundation Fellowship, the Reaumond Family Foundation, the Mark Foundation, the Childress Family Foundation, the McNair Family Foundation, and generous philanthropic contributions to the University of Texas MD Anderson Moon Shots Program. This work was also supported by the NIH/NCI Cancer Center Support Grants (CCSG P30CA016672), which supports MDACC's Small Animal Imaging Facility, Sequencing and Microarray Facility, and Research Histology Core Lab.

Acknowledgments

Graphical abstract created with BioRender.com adapted from the "Untargeted Metabolomics for Discover of Disease Biomarkers" template by Anne-Laure Agrinier (2021) retrieve from https://app.biorender.com/biorender-templates.

Conflicts of Interest:

C.M.T. was on the clinical advisory board of Accuray during the conduct of the study, has a patent for oral amifostine as a radioprotectant of the upper GI tract issues,

licensed, and with royalties paid from Xerient Pharmaceuticals and PHD inhibitors as a radioprotectant of the GI tract pending, and was the lead principal investigator of a multicenter trial testing the effects of high-dose SBRT with the radiomodulator, GC4419. All other authors declare no conflicts of interest.

References

1. Yu, M.; Nguyen, N.D.; Huang, Y.; Lin, D.; Fujimoto, T.N.; Molkentine, J.M.; Deorukhkar, A.; Kang, Y.; San Lucas, F.A.; Fernandes, C.J.; et al. Mitochondrial Fusion Exploits a Therapeutic Vulnerability of Pancreatic Cancer. *JCI Insight 4*, doi:10.1172/jci.insight.126915.
2. Hollinshead, K.E.R.; Parker, S.J.; Eapen, V.V.; Encarnacion-Rosado, J.; Sohn, A.; Oncu, T.; Cammer, M.; Mancias, J.D.; Kimmelman, A.C. Respiratory Supercomplexes Promote Mitochondrial Efficiency and Growth in Severely Hypoxic Pancreatic Cancer. *Cell Rep.* **2020**, *33*, 108231, doi:10.1016/j.celrep.2020.108231.
3. Zhao, J.; Zhang, J.; Yu, M.; Xie, Y.; Huang, Y.; Wolff, D.W.; Abel, P.W.; Tu, Y. Mitochondrial Dynamics Regulates Migration and Invasion of Breast Cancer Cells. *Oncogene* **2013**, *32*, 4814–4824, doi:10.1038/onc.2012.494.
4. Kashatus, J.A.; Nascimento, A.; Myers, L.J.; Sher, A.; Byrne, F.L.; Hoehn, K.L.; Counter, C.M.; Kashatus, D.F. Erk2 Phosphorylation of Drp1 Promotes Mitochondrial Fission and MAPK-Driven Tumor Growth. *Mol. Cell* **2015**, *57*, 537–551, doi:10.1016/j.molcel.2015.01.002.
5. Senft, D.; Ronai, Z.A. Regulators of Mitochondrial Dynamics in Cancer. *Curr. Opin. Cell Biol.* **2016**, *39*, 43–52, doi:10.1016/j.ceb.2016.02.001.
6. Koundinya, M.; Sudhalter, J.; Courjaud, A.; Lionne, B.; Touyer, G.; Bonnet, L.; Menguy, I.; Schreiber, I.; Perrault, C.; Vougier, S.; et al. Dependence on the Pyrimidine Biosynthetic Enzyme DHODH Is a Synthetic Lethal Vulnerability in Mutant KRAS-Driven Cancers. *Cell Chem. Biol.* **2018**, *25*, 705-717.e11, doi:10.1016/j.chembiol.2018.03.005.
7. Nagdas, S.; Kashatus, J.A.; Nascimento, A.; Hussain, S.S.; Trainor, R.E.; Pollock, S.R.; Adair, S.J.; Michaels, A.D.; Sesaki, H.; Stelow, E.B.; et al. Drp1 Promotes KRas-Driven Metabolic Changes to Drive Pancreatic Tumor Growth. *Cell Rep.* **2019**, *28*, 1845-1859.e5, doi:10.1016/j.celrep.2019.07.031.
8. Fujimoto, T.N.; Colbert, L.E.; Huang, Y.; Molkentine, J.M.; Deorukhkar, A.; Baseler, L.; Bonilla, M. de la C.; Yu, M.; Lin, D.; Gupta, S.; et al. Selective EGLN Inhibition Enables Ablative Radiotherapy and Improves Survival in Unresectable Pancreatic Cancer. *Cancer Res.* **2019**, *79*, 2327–2338, doi:10.1158/0008-5472.CAN-18-1785.

9. Yuan, M.; Breitkopf, S.B.; Yang, X.; Asara, J.M. A Positive/Negative Ion–Switching, Targeted Mass Spectrometry–Based Metabolomics Platform for Bodily Fluids, Cells, and Fresh and Fixed Tissue. *Nat. Protoc.* **2012**, *7*, 872–881, doi:10.1038/nprot.2012.024.
10. Sousa, C.M.; Biancur, D.E.; Wang, X.; Halbrook, C.J.; Sherman, M.H.; Zhang, L.; Kremer, D.; Hwang, R.F.; Witkiewicz, A.K.; Ying, H.; et al. Pancreatic Stellate Cells Support Tumour Metabolism through Autophagic Alanine Secretion. *Nature* **2016**, *536*, 479–483, doi:10.1038/nature19084.
11. Weckmann, K.; Diefenthäler, P.; Baeken, M.W.; Yusifli, K.; Turck, C.W.; Asara, J.M.; Behl, C.; Hajieva, P. Metabolomics Profiling Reveals Differential Adaptation of Major Energy Metabolism Pathways Associated with Autophagy upon Oxygen and Glucose Reduction. *Sci. Rep.* **2018**, *8*, 2337, doi:10.1038/s41598-018-19421-y.
12. Gao, J.; Guo, Z.; Cheng, J.; Sun, B.; Yang, J.; Li, H.; Wu, S.; Dong, F.; Yan, X. Differential Metabolic Responses in Breast Cancer Cell Lines to Acidosis and Lactic Acidosis Revealed by Stable Isotope Assisted Metabolomics. *Sci. Rep.* **2020**, *10*, 21967, doi:10.1038/s41598-020-78955-2.
13. Oza, V.H.; Aicher, J.K.; Reed, L.K. Random Forest Analysis of Untargeted Metabolomics Data Suggests Increased Use of Omega Fatty Acid Oxidation Pathway in Drosophila Melanogaster Larvae Fed a Medium Chain Fatty Acid Rich High-Fat Diet. *Metabolites* **2018**, *9*, E5, doi:10.3390/metabo9010005.
14. Graham, S.F.; Rey, N.L.; Yilmaz, A.; Kumar, P.; Madaj, Z.; Maddens, M.; Bahado-Singh, R.O.; Becker, K.; Schulz, E.; Meyerdirk, L.K.; et al. Biochemical Profiling of the Brain and Blood Metabolome in a Mouse Model of Prodromal Parkinson's Disease Reveals Distinct Metabolic Profiles. *J. Proteome Res.* **2018**, *17*, 2460–2469, doi:10.1021/acs.jproteome.8b00224.
15. Liang, J.; Yang, Y.; Bai, L.; Li, F.; Li, E. DRP1 Upregulation Promotes Pancreatic Cancer Growth and Metastasis through Increased Aerobic Glycolysis. *J. Gastroenterol. Hepatol.* **2020**, *35*, 885–895, doi:10.1111/jgh.14912.
16. Matoba, S.; Kang, J.-G.; Patino, W.D.; Wragg, A.; Boehm, M.; Gavrilova, O.; Hurley, P.J.; Bunz, F.; Hwang, P.M. P53 Regulates Mitochondrial Respiration. *Science* **2006**, *312*, 1650–1653, doi:10.1126/science.1126863.
17. Catchpole, G.; Platzer, A.; Weikert, C.; Kempkensteffen, C.; Johannsen, M.; Krause, H.; Jung, K.; Miller, K.; Willmitzer, L.; Selbig, J.; et al. Metabolic Profiling Reveals Key Metabolic Features of Renal Cell Carcinoma. *J. Cell. Mol. Med.* **2011**, *15*, 109–118, doi:https://doi.org/10.1111/j.1582-4934.2009.00939.x.
18. Pelicano, H.; Xu, R.; Du, M.; Feng, L.; Sasaki, R.; Carew, J.S.; Hu, Y.; Ramdas, L.; Hu, L.; Keating, M.J.; et al. Mitochondrial Respiration Defects in Cancer Cells Cause Activation of Akt Survival Pathway through a Redox-Mediated Mechanism. *J. Cell Biol.* **2006**, *175*, 913–923, doi:10.1083/jcb.200512100.

19. Hardie, R.-A.; van Dam, E.; Cowley, M.; Han, T.-L.; Balaban, S.; Pajic, M.; Pinese, M.; Iconomou, M.; Shearer, R.F.; McKenna, J.; et al. Mitochondrial Mutations and Metabolic Adaptation in Pancreatic Cancer. *Cancer Metab.* **2017**, *5*, 2, doi:10.1186/s40170-017-0164-1.
20. Santana-Codina, N.; Roeth, A.A.; Zhang, Y.; Yang, A.; Mashadova, O.; Asara, J.M.; Wang, X.; Bronson, R.T.; Lyssiotis, C.A.; Ying, H.; et al. Oncogenic KRAS Supports Pancreatic Cancer through Regulation of Nucleotide Synthesis. *Nat. Commun.* **2018**, *9*, 4945, doi:10.1038/s41467-018-07472-8.
21. Ying, H.; Kimmelman, A.C.; Lyssiotis, C.A.; Hua, S.; Chu, G.C.; Fletcher-Sananikone, E.; Locasale, J.W.; Son, J.; Zhang, H.; Coloff, J.L.; et al. Oncogenic Kras Maintains Pancreatic Tumors through Regulation of Anabolic Glucose Metabolism. *Cell* **2012**, *149*, 656–670, doi:10.1016/j.cell.2012.01.058.
22. Vettore, L.; Westbrook, R.L.; Tennant, D.A. New Aspects of Amino Acid Metabolism in Cancer. *Br. J. Cancer* **2020**, *122*, 150–156, doi:10.1038/s41416-019-0620-5.
23. Bryant, K.L.; Mancias, J.D.; Kimmelman, A.C.; Der, C.J. KRAS: Feeding Pancreatic Cancer Proliferation. *Trends Biochem. Sci.* **2014**, *39*, 91–100, doi:10.1016/j.tibs.2013.12.004.
24. Viale, A.; Pettazzoni, P.; Lyssiotis, C.A.; Ying, H.; Sánchez, N.; Marchesini, M.; Carugo, A.; Green, T.; Seth, S.; Giuliani, V.; et al. Oncogene Ablation-Resistant Pancreatic Cancer Cells Depend on Mitochondrial Function. *Nature* **2014**, *514*, 628–632, doi:10.1038/nature13611.
25. Dey, P.; Li, J.; Zhang, J.; Chaurasiya, S.; Strom, A.; Wang, H.; Liao, W.-T.; Cavallaro, F.; Denz, P.; Bernard, V.; et al. Oncogenic KRAS-Driven Metabolic Reprogramming in Pancreatic Cancer Cells Utilizes Cytokines from the Tumor Microenvironment. *Cancer Discov.* **2020**, *10*, 608–625, doi:10.1158/2159-8290.CD-19-0297.
26. Efron, B.; Tibshirani, R.; Storey, J.D.; Tusher, V. Empirical Bayes Analysis of a Microarray Experiment. *J. Am. Stat. Assoc.* **2001**, *96*, 1151–1160, doi:10.1198/016214501753382129.
27. Jeanmougin, M.; Reynies, A. de; Marisa, L.; Paccard, C.; Nuel, G.; Guedj, M. Should We Abandon the T-Test in the Analysis of Gene Expression Microarray Data: A Comparison of Variance Modeling Strategies. *PLOS ONE* **2010**, *5*, e12336, doi:10.1371/journal.pone.0012336.
28. Zhang, S. A Comprehensive Evaluation of SAM, the SAM R-Package and a Simple Modification to Improve Its Performance. *BMC Bioinformatics* **2007**, *8*, 230, doi:10.1186/1471-2105-8-230.

29. Tusher, V.G.; Tibshirani, R.; Chu, G. Significance Analysis of Microarrays Applied to the Ionizing Radiation Response. *Proc. Natl. Acad. Sci. U. S. A.* **2001**, *98*, 5116–5121, doi:10.1073/pnas.091062498.
30. Worley, B.; Powers, R. Multivariate Analysis in Metabolomics. *Curr. Metabolomics* **2013**, *1*, 92–107, doi:10.2174/2213235X11301010092.
31. Yun, Y.-H.; Liang, F.; Deng, B.-C.; Lai, G.-B.; Vicente Gonçalves, C.M.; Lu, H.-M.; Yan, J.; Huang, X.; Yi, L.-Z.; Liang, Y.-Z. Informative Metabolites Identification by Variable Importance Analysis Based on Random Variable Combination. *Metabolomics* **2015**, *11*, 1539–1551, doi:10.1007/s11306-015-0803-x.
32. Chong, I.-G.; Jun, C.-H. Performance of Some Variable Selection Methods When Multicollinearity Is Present. *Chemom. Intell. Lab. Syst.* **2005**, *78*, 103–112, doi:10.1016/j.chemolab.2004.12.011.
33. Lin, Z.; Vicente Gonçalves, C.M.; Dai, L.; Lu, H.; Huang, J.; Ji, H.; Wang, D.; Yi, L.; Liang, Y. Exploring Metabolic Syndrome Serum Profiling Based on Gas Chromatography Mass Spectrometry and Random Forest Models. *Anal. Chim. Acta* **2014**, *827*, 22–27, doi:10.1016/j.aca.2014.04.008.
34. Poisson, L.M.; Munkarah, A.; Madi, H.; Datta, I.; Hensley-Alford, S.; Tebbe, C.; Buekers, T.; Giri, S.; Rattan, R. A Metabolomic Approach to Identifying Platinum Resistance in Ovarian Cancer. *J. Ovarian Res.* **2015**, *8*, 13, doi:10.1186/s13048-015-0140-8.
35. Pang, Z.; Chong, J.; Zhou, G.; de Lima Morais, D.A.; Chang, L.; Barrette, M.; Gauthier, C.; Jacques, P.-É.; Li, S.; Xia, J. MetaboAnalyst 5.0: Narrowing the Gap between Raw Spectra and Functional Insights. *Nucleic Acids Res.* **2021**, *49*, W388–W396, doi:10.1093/nar/gkab382.
36. Blighe, K.; Rana, S.; Turkes, E.; Ostendorf, B.; Grioni, A.; Lewis, M. *EnhancedVolcano: Publication-Ready Volcano Plots with Enhanced Colouring and Labeling*; Bioconductor version: Release (3.13), 2021.

bioRxiv preprint doi: https://doi.org/10.1101/2021.08.06.455450; this version posted August 8, 2021. The copyright holder for this preprint (which was not certified by peer review) is the author/funder, who has granted bioRxiv a license to display the preprint in perpetuity. It is made available under aCC-BY-NC-ND 4.0 International license.

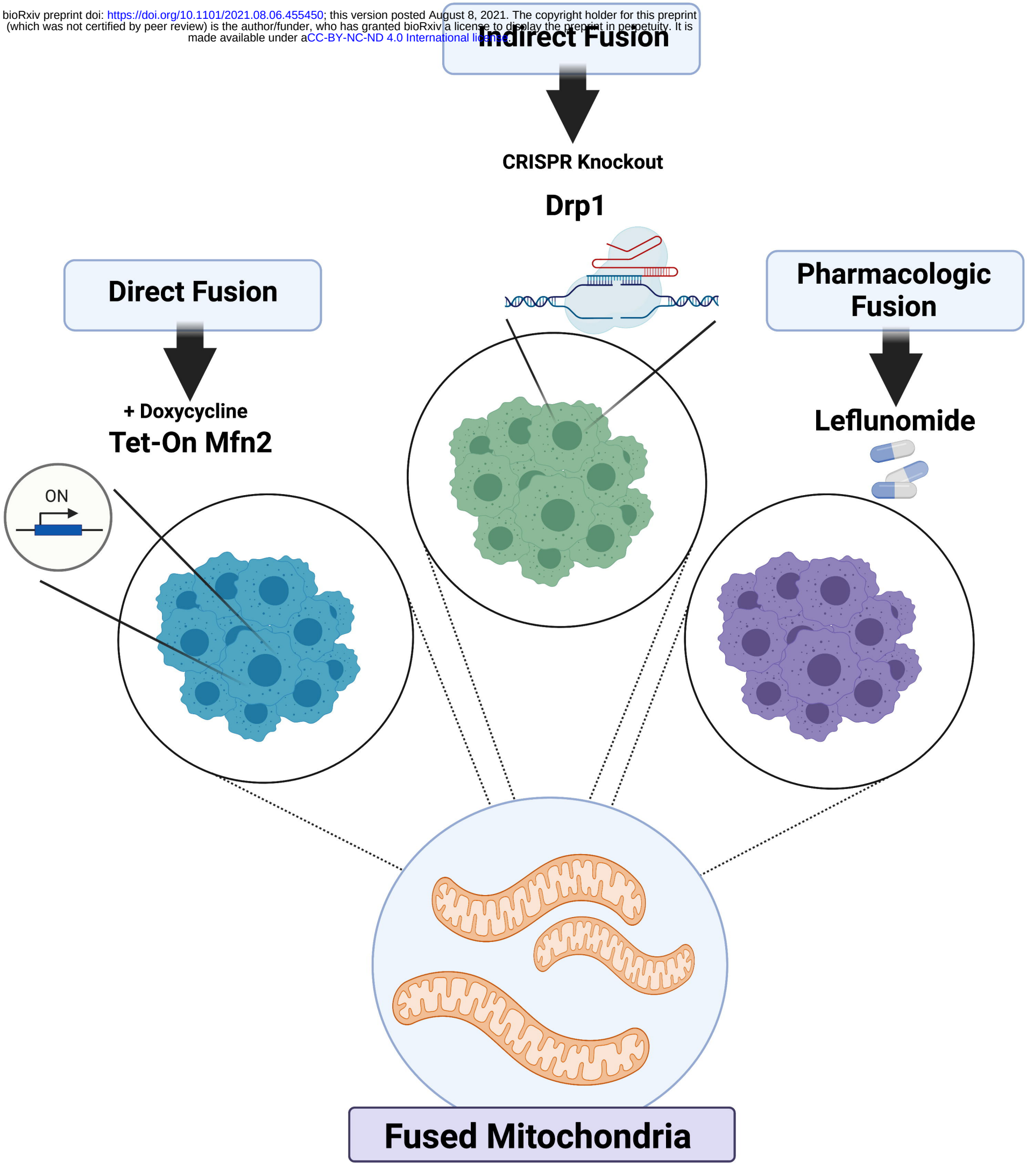

A

Tet-On Mfn2 (Direct Fusion) | **sgDrp1** (Indirect Fusion) | **Leflunomide** (Pharmacologic)

Supervised Clustering

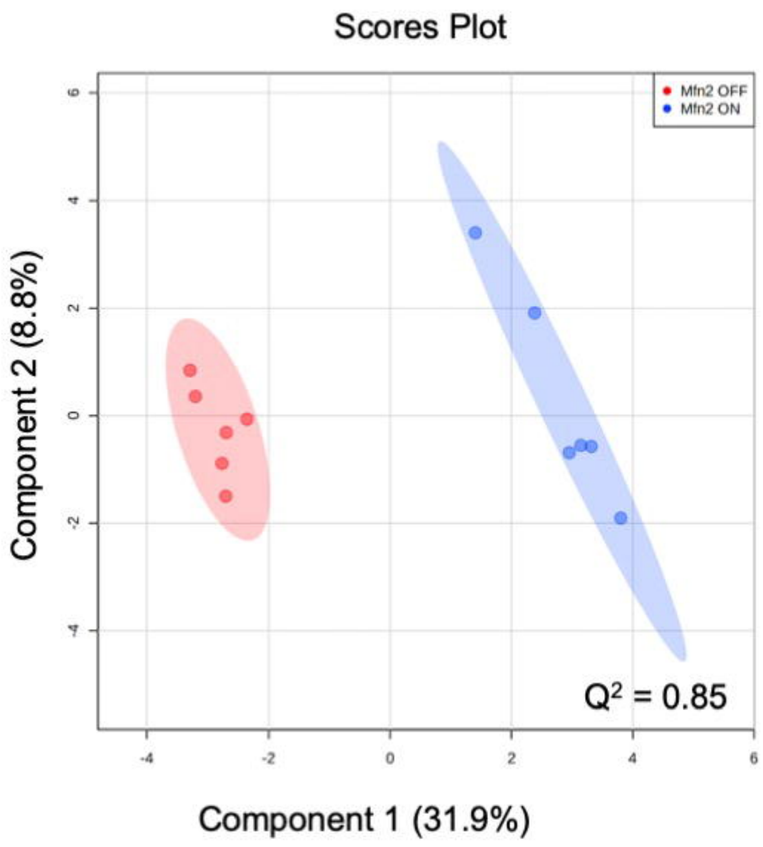

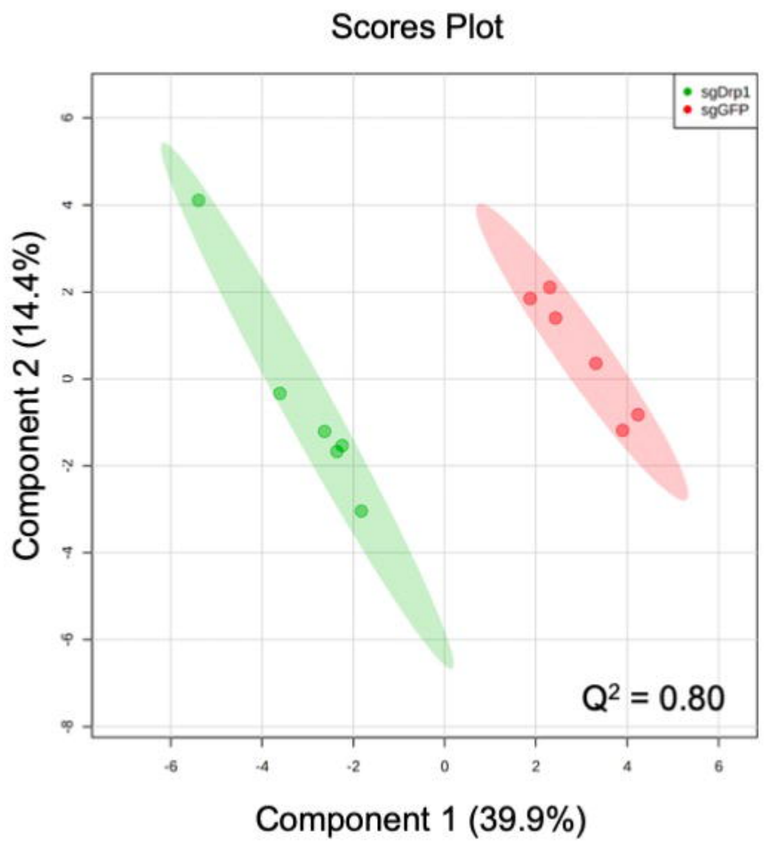

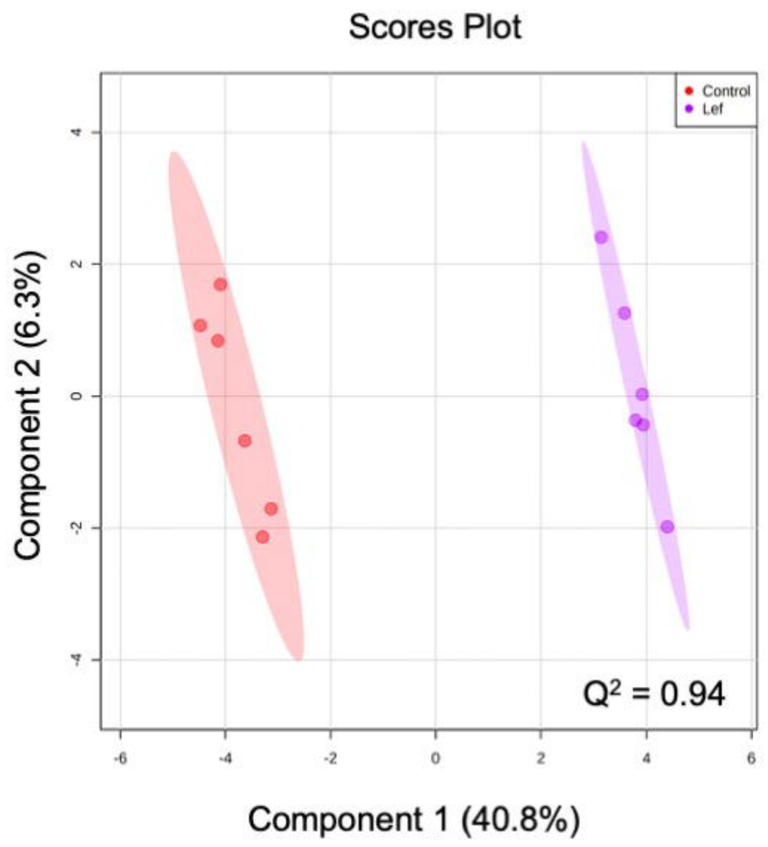

B

Unsupervised Clustering

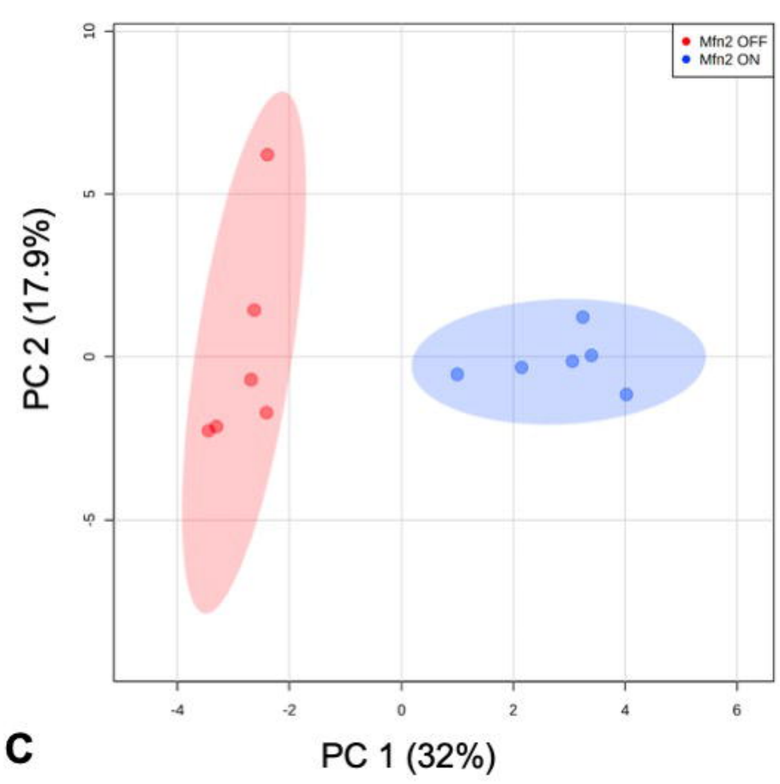

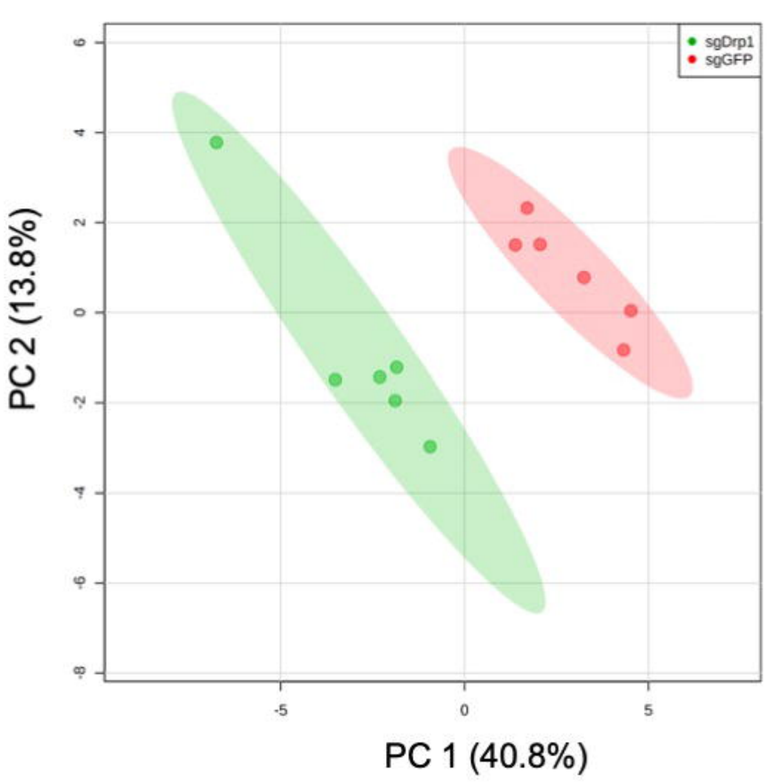

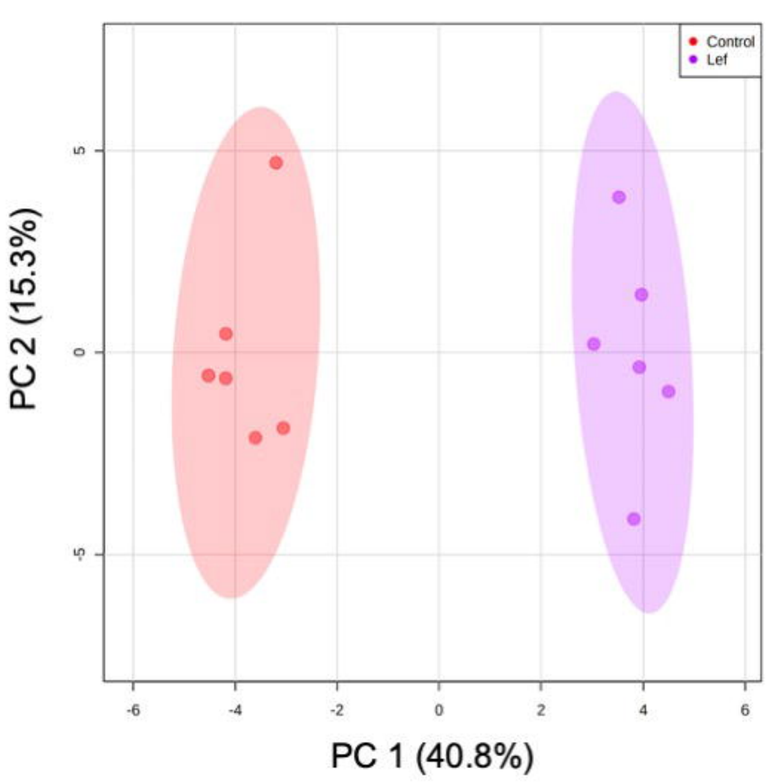

C

bioRxiv preprint doi: https://doi.org/10.1101/2021.08.06.455450; this version posted August 8, 2021. The copyright holder for this preprint (which was not certified by peer review) is the author/funder, who has granted bioRxiv a license to display the preprint in perpetuity. It is made available under aCC-BY-NC-ND 4.0 International license.

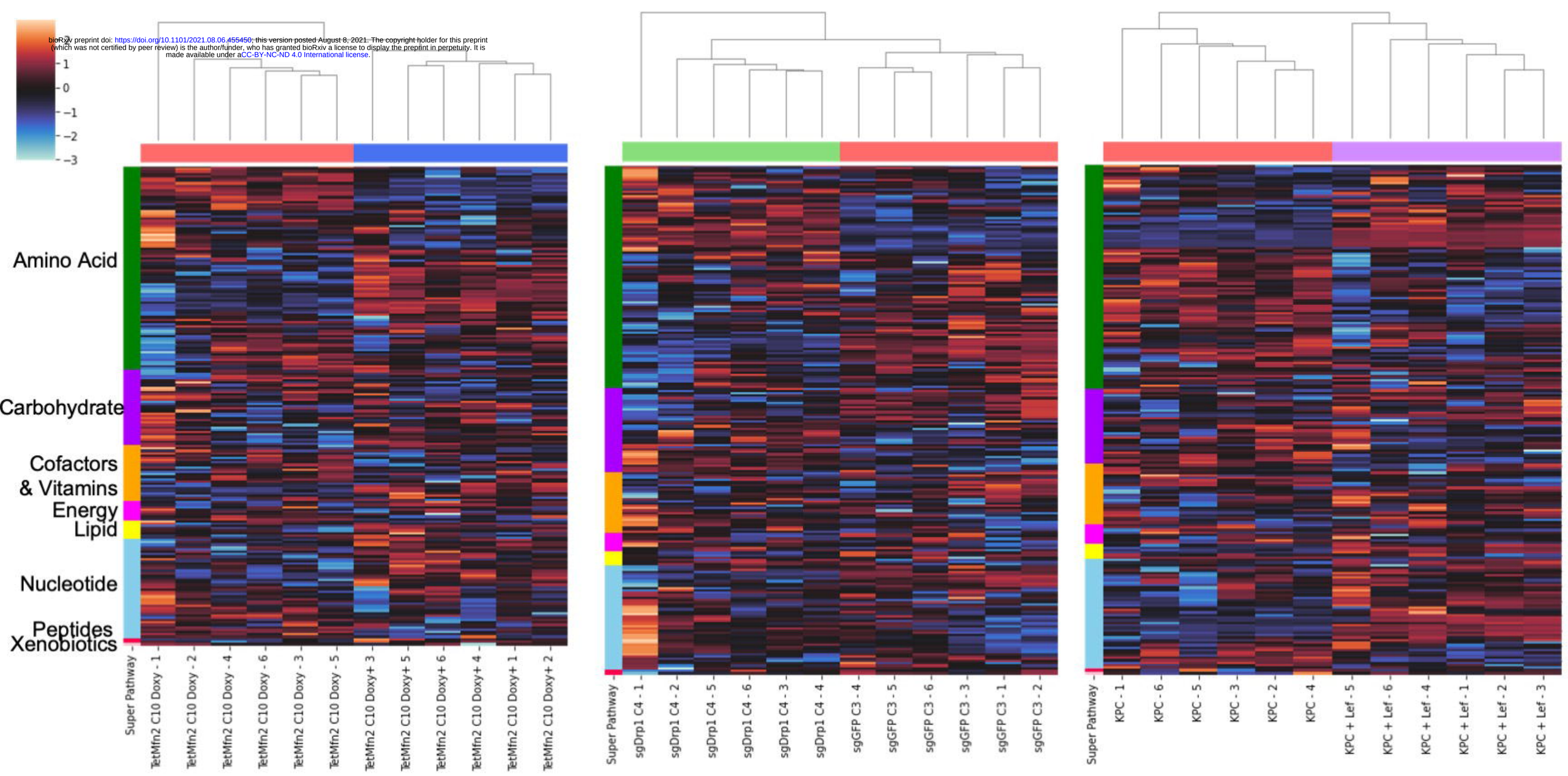

Direct Fusion

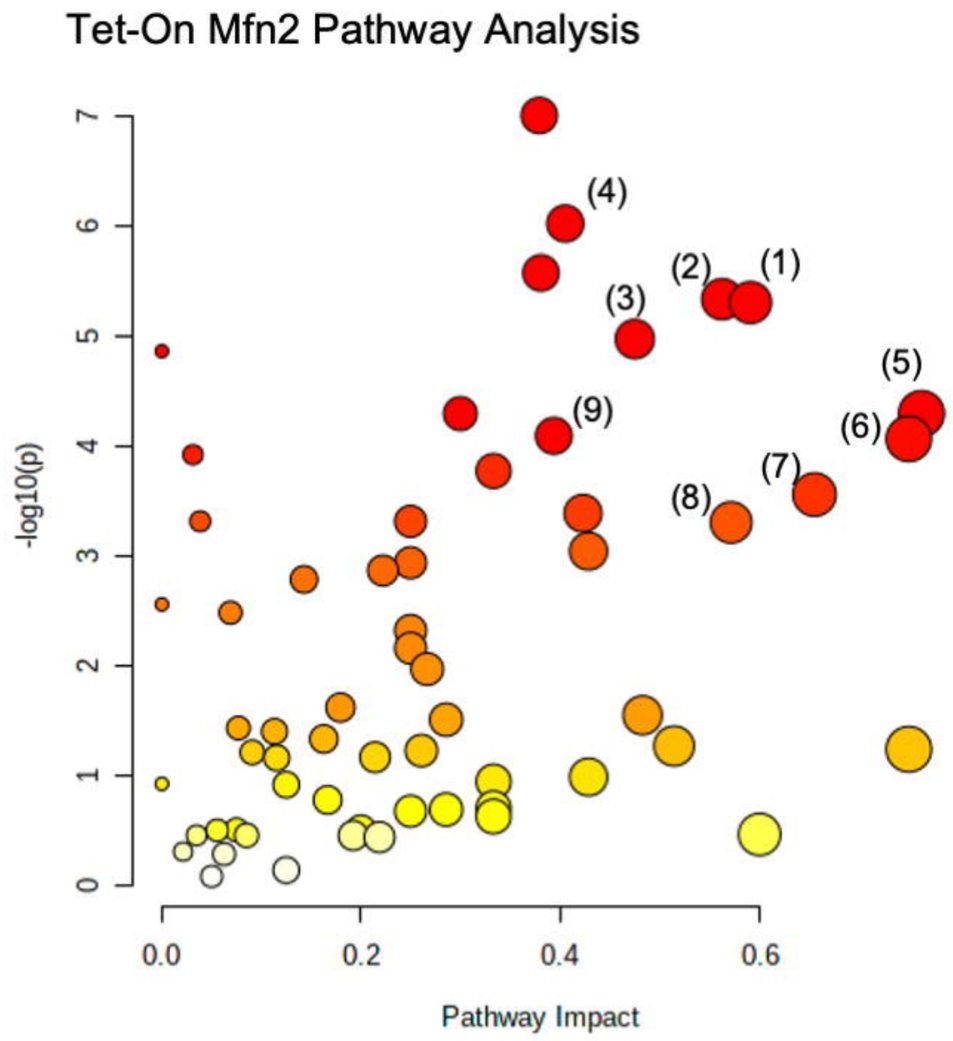

(1) Purine Metabolism
(2) Alanine, Aspartate, and Glutamate Metabolism
(3) Arginine and Proline Metabolism
(4) Glutathione Metabolism
(5) Pyrimidine Metabolism
(6) Arginine Biosynthesis
(7) Pentose Phosphate Pathway
(8) Nicotinate and Nicotinamide metabolism
(9) Cysteine and Methionine metabolism

Indirect Fusion

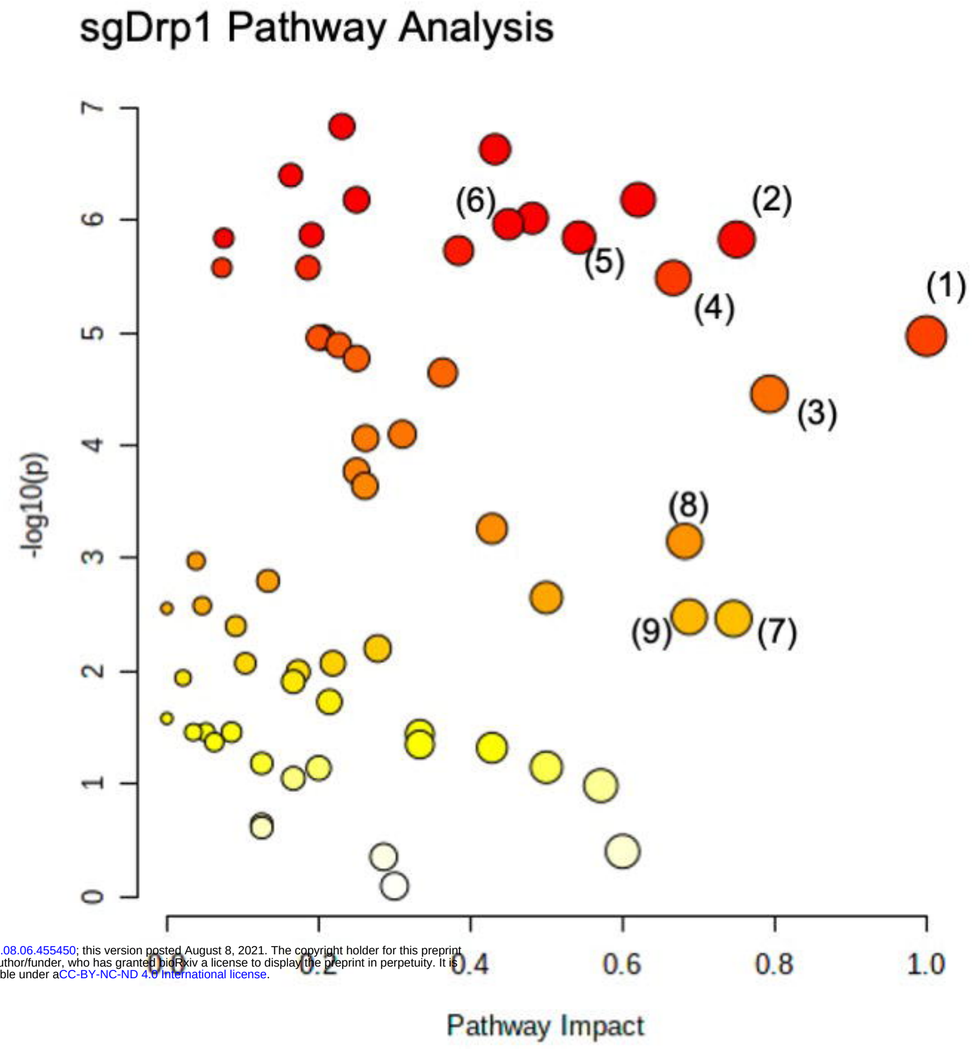

(1) Synthesis and Degradation of Ketone Bodies
(2) Alanine, Aspartate, and Glutamate Metabolism
(3) Pentose Phosphate Pathway
(4) Butanoate Metabolism
(5) Glycolysis/ Gluconeogenesis
(6) Arginine and Proline Metabolism
(7) Pyrimidine Metabolism
(8) Purine Metabolism
(9) Arginine Biosynthesis

bioRxiv preprint doi: https://doi.org/10.1101/2021.08.06.455450; this version posted August 8, 2021. The copyright holder for this preprint (which was not certified by peer review) is the author/funder, who has granted bioRxiv a license to display the preprint in perpetuity. It is made available under aCC-BY-NC-ND 4.0 International license.

Pharmacologic Fusion

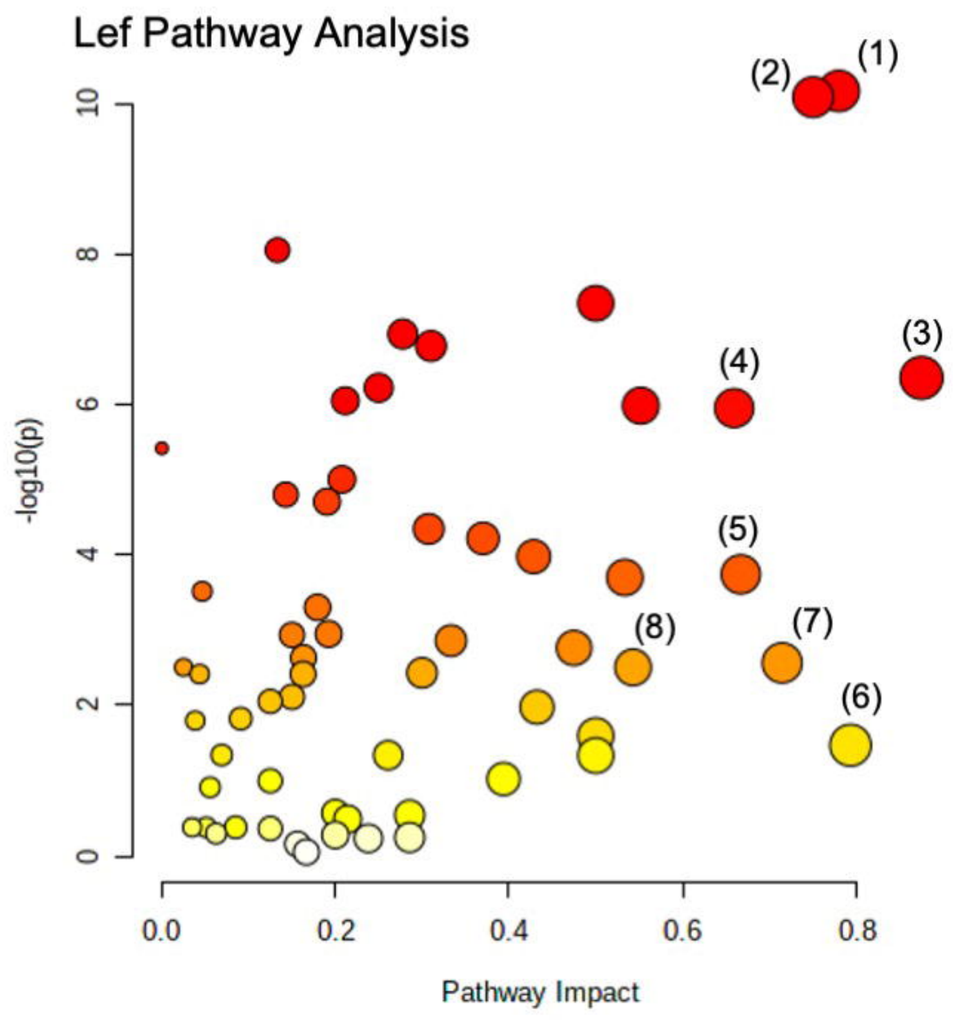

(1) Pyrimidine Metabolism
(2) Alanine, Aspartate, and Glutamate Metabolism
(3) Arginine Biosynthesis
(4) Purine Metabolism
(5) Nicotinate and Nicotinamide metabolism
(6) Pentose Phosphate Pathway
(7) Synthesis and degradation of Ketone Bodies
(8) Glycolysis/ Gluconeogenesis

Tet-On Mfn2 (Direct Fusion)

sgDrp1 (Indirect Fusion)

Leflunomide (Pharmacologic)

A

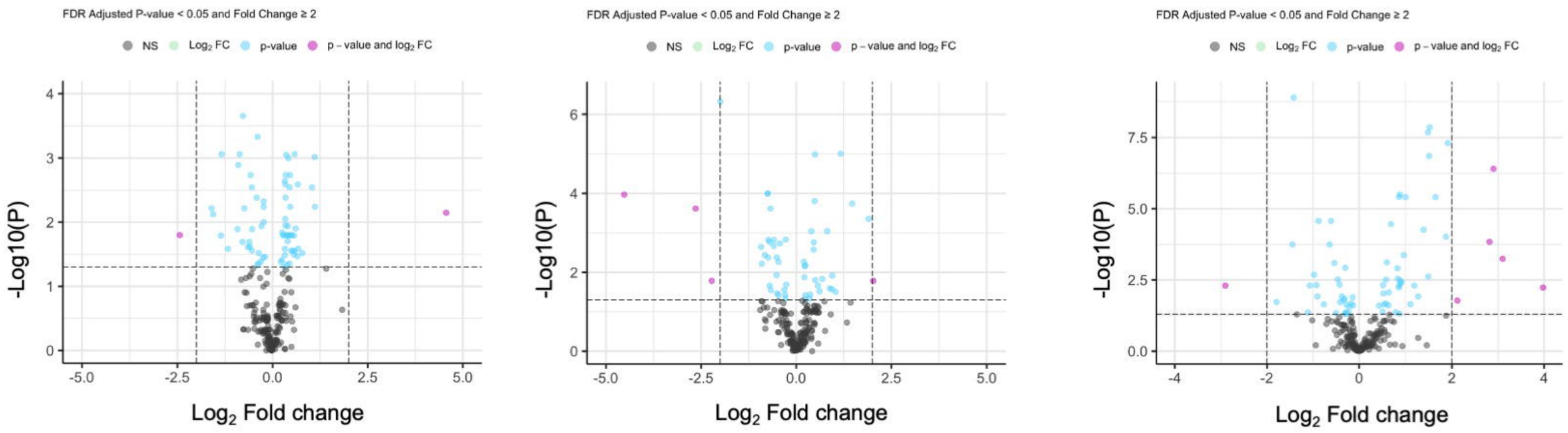

B

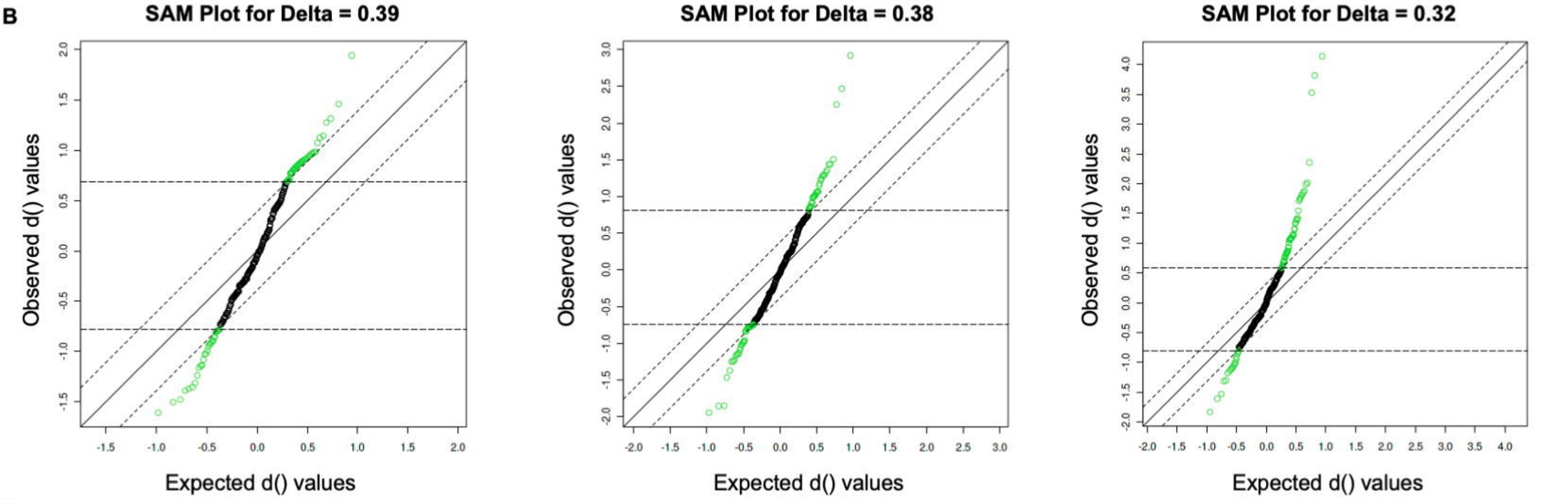

C

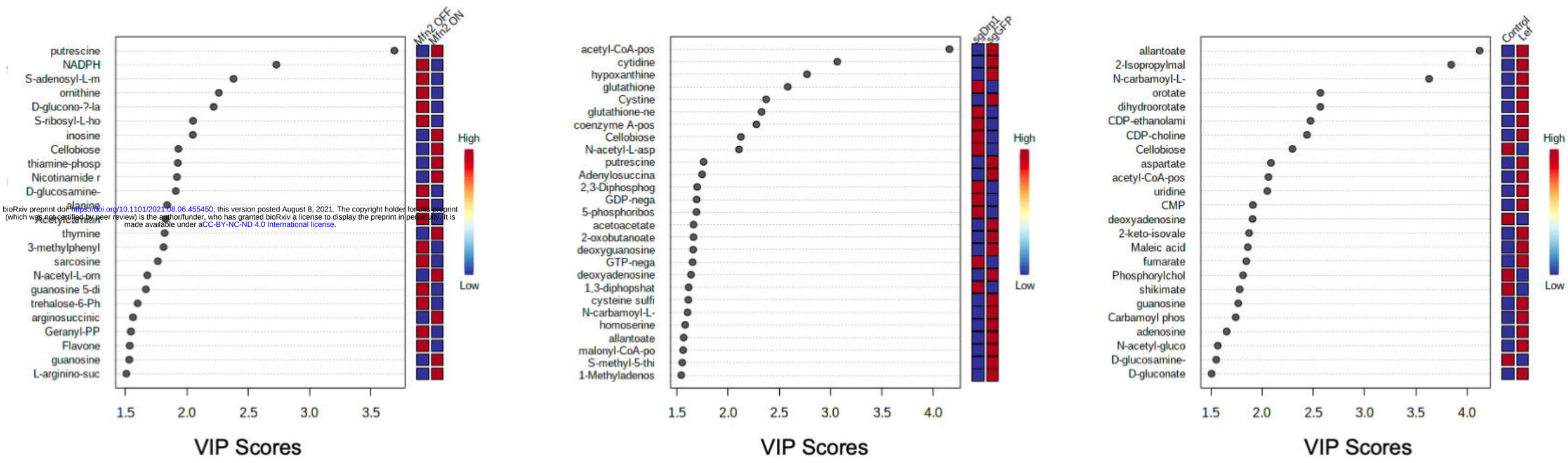

D

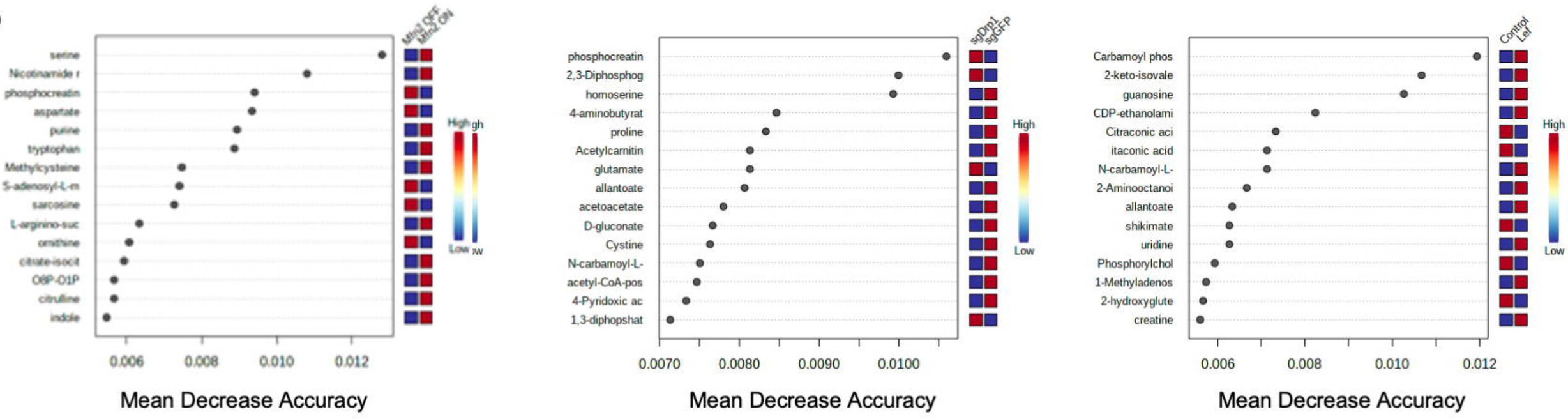

bioRxiv preprint doi: https://doi.org/10.1101/2021.08.06.455450; this version posted August 8, 2021. The copyright holder for this preprint (which was not certified by peer review) is the author/funder, who has granted bioRxiv a license to display the preprint in perpetuity. It is made available under aCC-BY-NC-ND 4.0 International license.

Tet-On Mfn2 Pathway Analysis

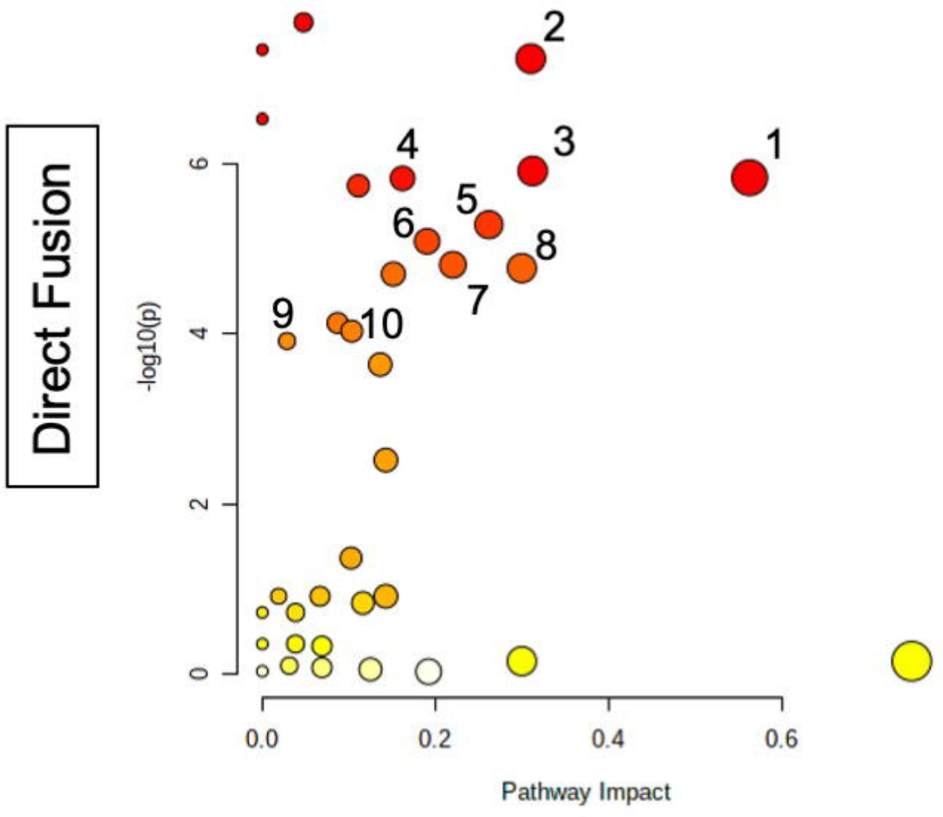

1. Arginine Biosynthesis
2. Aminoacyl-tRNA Biosynthesis
3. Alanine, Aspartate, and Glutamate Metabolism
4. Glutathione Metabolism
5. Glycine, Serine, and Threonine Metabolism
6. Nicotinate and Nicotinamide Metabolism
7. Pyrimidine Metabolism
8. Arginine and Proline Metabolism
9. Glycolysis/Gluconeogenesis
10. Pentose Phosphate Pathway

sgDrp1 Pathway Analysis

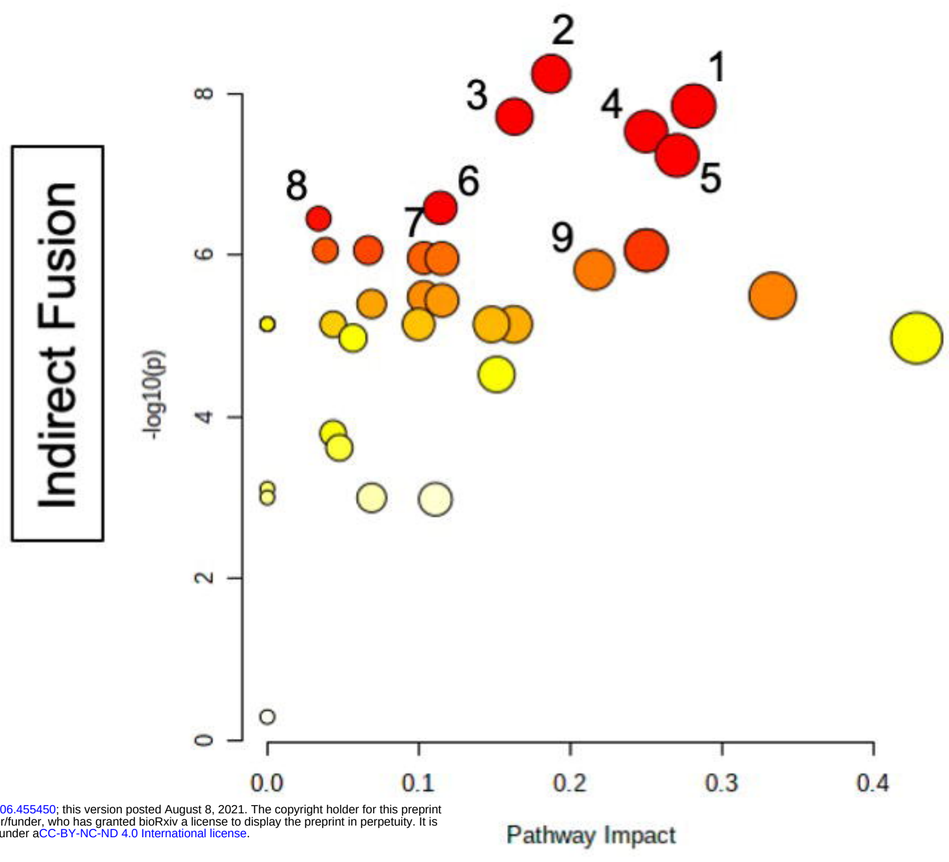

1. Alanine, Aspartate, and Glutamate Metabolism
2. Arginine Biosynthesis
3. Fatty Acid Degradation
4. Arginine and Proline Metabolism
5. Glutathione Metabolism
6. Glycolysis/Gluconeogenesis
7. Pentose Phosphate Pathway
8. Pyrimidine Metabolism
9. Purine Metabolism

bioRxiv preprint doi: https://doi.org/10.1101/2021.08.06.455450; this version posted August 8, 2021. The copyright holder for this preprint (which was not certified by peer review) is the author/funder, who has granted bioRxiv a license to display the preprint in perpetuity. It is made available under aCC-BY-NC-ND 4.0 International license.

Lef Pathway Analysis

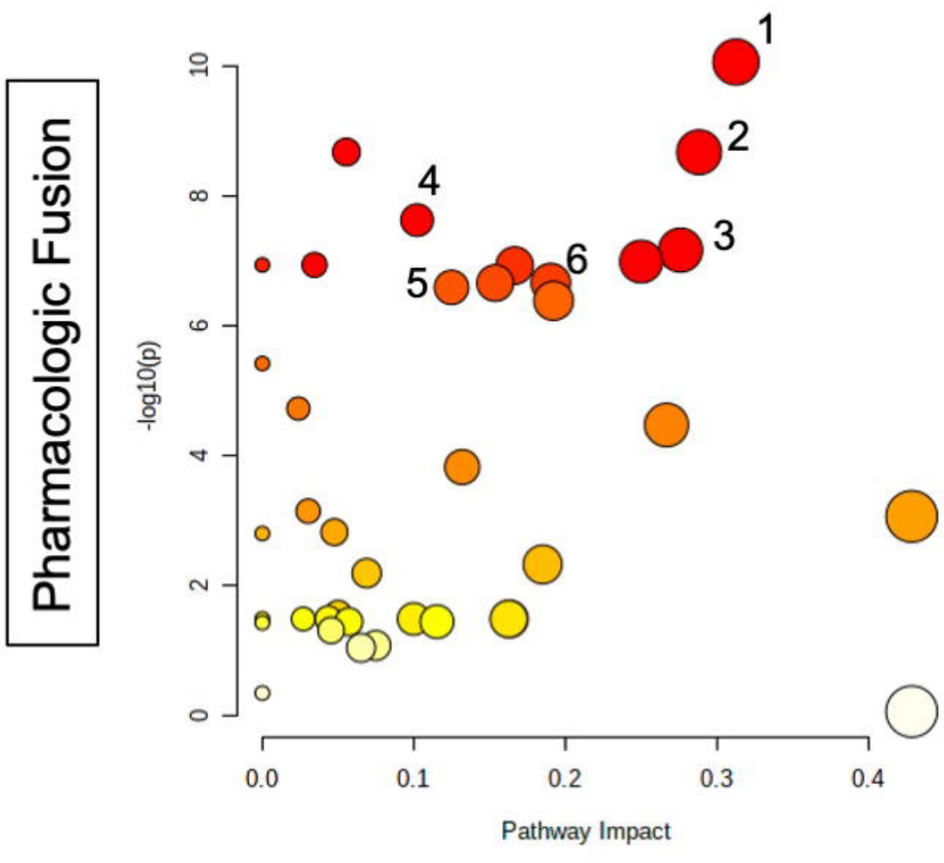

1. Alanine, Aspartate, and Glutamate Metabolism
2. Pyrimidine Metabolism
3. TCA Cycle
4. Purine Metabolism
5. Arginine Biosynthesis
6. Nicotinate and Nicotinamide Metabolism